THESIS

BED SEDIMENT TRANSPORT AND CHANNEL MORPHOLOGY IN A BRAIDED CHANNEL: INSIGHTS FROM A FLUME EXPERIMENT

Submitted by

Dylan L. Armstrong

Department of Civil and Environmental Engineering

In partial fulfillment of the requirements

For the Degree of Master of Science

Colorado State University

Fort Collins, Colorado

Spring 2017

Master's Committee:

Advisor: Robert Ettema

Peter Nelson
Michael Falkowski

ABSTRACT

BED SEDIMENT TRANSPORT AND CHANNEL MORPHOLOGY IN A BRAIDED CHANNEL: INSIGHTS FROM A FLUME EXPERIMENT

This thesis presents the methods and findings from an experiment aimed at relating the rate of bed-sediment transport through a reach of a braided channel to the intensity of the braiding sub-channels (anabranches) along the reach. The experiment was conducted in a large flume located at Colorado State University's Hydraulics Laboratory in Fort Collins, Colorado. No similar flume experiments have been conducted involving braided channels in a wide alluvial plain. Such experiments involve several challenging considerations that greatly complicate such experiments: braided channels are characteristically wide and shallow; have relatively large bed-sediment loads that are difficult to measure, because they move in multiple sub-channels; and the sub-channels (often termed anabranches) are ephemeral. The self-forming nature of the anabranches means that there is little direct control over the exact morphology of the braided channel. The objectives set forth in this experiment overcame the challenges of braided river flume studies, and allowed a comprehensive data set to be obtained of both bed sediment transport data and morphologic braided intensity data. The intensity of braiding was characterized using a braiding index (Flow Width Ratio) developed during this experiment. A relationship was identified and a trend established – as FWR increased, the rate of bed-sediment transport decreased – but the stochastic nature of transport rates and morphology introduced much scatter in the relationship. It was found that local morphologic features have a large impact on the transport of sediment through braided systems, and that the features could help explain some of the scatter in the data.

ACKNOWLEGMENTS

I would like to thank the Colorado State Universities Hydraulics Laboratory and the staff for allowing me conduct my experiment and for their continued support and dedication to research. I would also like to thank; my advisor, Dr. Robert Ettema for his uplifting spirit, positive encouragement, and continued support throughout the experiment; my committee members Dr. Peter Nelson and Dr. Michael Falkowski for their advice and help throughout the experiment. Also, I would like to thank all the faculty at Colorado State Universities Civil and Environmental Engineering department who have inspired my passion for work and research the field of hydraulics engineering. Lastly, I want to thank my family, friends, and fellow graduate students for their kindness, expertise, and support throughout this experiment and my graduate career in general.

TABLE OF CONTENTS

LIST OF TABLES

LIST OF FIGURES

1. Introduction

1.1 Background

This study used a large flume that enabled a braided channel system to develop over a plane of uniform sediment that was relatively wide and long compared to typical widths and depths of sub-channels or anabranches forming the braided channel. The design of the experiment included a sloped chute at the downstream boundary that facilitated the collection and measurement of bed sediment outflow from the model. The data on sediment outflow were compared with data on braiding morphology recorded by means of photogrammetric techniques and LiDAR technology. The comparison revealed useful insights as to how bed-sediment transport relates to braided-channel morphology, and allowed for spatial and temporal examination of the evolution of certain morphological mechanisms involved in braided-channel dynamics.

The motivation for this research stemmed from an Army Corps of Engineers hydraulics model study of the reach of the North Fork of the Toutle River, in the state of Washington. The study, conducted at Colorado State University's Hydraulics Laboratory, involved investigating the performance of alternative structures for retaining bed sediment along a reach heavily affected by the 1980 Mount Saint Helens eruption. During the eruption, the largest recorded terrestrial landslide in history occurred and deposited an estimated 2.5 cubic kilometers of material (USGS). The majority of the sediment released in the eruption was contained in the upper section of the North Fork Toutle River by a sediment retention structure, a large dam that was especially built for this purpose, which has since been filled with sediment. The dam formed an extensive depositional, sediment plain that extends for miles upstream from the dam. Figure 1 shows the plain and the braided river system that has formed subsequently over it.

The modeling of the sediment-retention structures involved a unique series of experiments conducted with the large, wide flume so as to replicate the unsteady aspects of braided channel morphology and bed sediment transport. During the course of the testing it became apparent that sediment transport through the braided system was unsteady and dynamic in nature. An observation was made that the flux of sediment seemed to coincide with observed morphologic features of the braided system, which continually adjusted with time. The present experiment was planned to examine this observation and to reveal more about the little studied sediment transport through such systems. The experiment proved to be challenging in several ways, including the selection or development of effective methods of data collection. This thesis presents findings as well as the methods used and describes how they were useful for relating sediment transport to the morphology of a braided channel.

Figure 1: A view of the sediment plain extending upstream from the sediment retention structure with Mount Saint Helens in the far distance (Source: CENWP 2013)

1.2 Objectives and Approach

Early work with the braided channels formed in the flume revealed a possible correlation between the morphology of the braided system and the sediment transport through the system. It was concluded that this correlation could be shown by measuring the rate of sediment outflow while simultaneously measuring an indicator of channel condition (such as a braided intensity index) determined via photographic methods. The time-histories of sediment transport and channel morphology provide a useful insight into the dynamic behavior of a braided channel. In accordance with investigating the relationship, this thesis had the following specific objectives:

1. Establish the parameters and procedure for establishing a braided channel along a flume;
2. Determine effective methods for measuring and relating bed-sediment transport and braided-channel morphology; and,
3. Ascertain how rate of bed sediment transport out of the reach contained along the flume relates to the morphology of the braided channel.

2. Literature Review

2.1 Braided Rivers

The knowledge of braided rivers over the last couple decades has increased significantly (e.g., Smith. G. S. 2006). This advance is due to recent improvements in surveying and remote sensing technology. However, there are still a lot of questions to be answered involving braided rivers. According to Best et al. (2006), "more experimental work should be devoted to understanding bifurcations and other mechanisms in generating the complex structures of braided rivers." A major mechanism involved in controlling the complexities of braided systems is the rate of bed-sediment transport throughout the braided channel. However, collecting sediment transport data in a braided river is greatly complicated by the multitude and the dynamic nature of sub-channels or anabranches. Moreover, a substantial difficulty is attempting to record the changing state of the anabranches while measuring bed-sediment transport over a period of time.

Few studies have attempted to correlate sediment fluxes and morphology of braided channels. The results to date are rather mixed. Ashmore (2002), Bezzola and Marti (2006), and Warburton (1996) all produced findings that conclude a higher braided index, a measure of braided intensity over a reach, correlates to a lower sediment flux through a system. Opposing results were found by Warburton and Davies (1994). It is possible that the contrasting conclusions could have resulted from different periods of aggradation or degradation, as suggested by Smith (2006).

Extensive literature on braided-channel networks exists. Sambrook at al. (2006) give a useful summary of the literature and sense of the state of knowledge about braided-channel networks. A sample of other notable references are Peale (1877), Howard et al. (1972), Ashmore (1981), Graf (1981), Hoey and

Sutherland (1991), Rinaldo and Rodriguez-Iturbe (1993), Warburton and Davies (1994), and Bertoldi et al. (2014). Pertinent insights drawn from the literature include:

1. They typically form on bed or valley slopes steeper than most do other alluvial channel morphologies;
2. Braided-channel networks or systems commonly are in a state of dynamic equilibrium, whereby their channel morphology and bed sediment transport tend to be unsteady, varying about temporal mean values. This characteristic is often described in terms of channel instability;
3. Braided channels can be highly complex in morphology, and are more usefully described in terms of spatial mean values as well as temporal mean values. Statistical, self-organization and fractal concepts are occasionally applied to braided-channel networks to explain their morphologic behavior;
4. Considerable discussion revolves around how to characterize braided-channel morphology. One metric often mentioned is braiding index, which counts the mean number of active channels or braid bars per river transect;
5. Laboratory flume experiments are largely limited to flumes less than about 10ft wide, such that lateral shifting of channels is rather constrained. Most studies have involved flume widths 6ft or less;
6. A topic of current research involves the effects of vegetation on channel morphology and stability; and,
7. Field measurement of bed sediment transport in braided-channel networks is made difficult by the need to measure transport rates almost simultaneously in multiple channels.

The present hydraulic experiment ventures into a region of mobile-bed hydrodynamics where the relationships among water discharge , rate of sediment transport, channel slope, and channel morphology are less understood than most other aspects of mobile-bed hydraulics.

2.2 Moveable-bed Hydraulic Models

To date, few physical modeling projects have involved a self-forming braided network in a wide alluvial plain (Ettema et al. 2016). A contributing consideration has been the relative scarcity of large flumes suitably long and wide. It is useful to review concepts of mobile-bed modeling to understand how this experiment would project itself to a real sized braided river. This part of the literature review covers the main considerations associated with the design and use of moveable-bed models to simulate bed sediment movement and accumulation along a large alluvial channel, especially a wide braided morphology such as the experiments based project site. The following considerations guide the design, operation, and interpretation of the moveable-bed model for the present project and, therefore, are of particular interest for this review:

1. There must be active bedload transport of the model bed sediment. Bed sediment mobility, intensity of transport, and patterns of accumulation are key processes;
2. Flow and bedload transport must produce a braided-channel network having a similar planform as observed for a range of flows at the project site for a good reference;

The review consulted numerous reference sources, including general references on moveable-bed modeling, including the following sources: Allen (1952), Einstein and Chien (1954), Gessler (1971), Franco (1978), Hudson et al. (1979), ASCE (2000), Kobus (1980), Martins (1989), Shen (1990), Hughes (1993), Yen (1999), Julien (2002), and Pugh (2008). Few references describe moveable-bed modeling of large braided channels. Of these studies, the one closest to describing a channel similar to the present project is the study reported for the Jamuna River by Klaassen (1990, 1992) and Moreton et al. (2002). The main insights from prior moveable-bed models of large channels are as follow:

1. Several approaches have been used to design and operate models, such as the proposed experiment:

i. The "basic approach" founded on Froude number similitude with the Shields number similitude condition used to ensure a representative level of bed sediment mobility and reasonable replication of channel morphology (e.g., ASCE 2000);

ii. An alternative approach aimed expressly at accurate simulation of bedload transport (Einstein and Chien 1954; ASCE 2000; Pugh 2008); and,

iii. A "hybrid approach" used by Delft Hydraulics for modeling a reach of the Jamuna River (Klaassen 1990); and

iv. The "USACE approach" proceeding from similitude of channel size and morphology (Franco 1978).

Approaches i and ii rely on the use of semi-empirical relationships for hydraulic geometry.

2. Modelers have used three approaches to satisfy similitude requirements for turbulent flow and bedload movement:

   i. Vertical distortion to ensure turbulent flow;

   ii. Light-weight model sediment to ensure sediment mobility; and,

   iii. Supplementary slope to increase hydrodynamic force on the model bed.

3. Many models of large channels are vertically distorted, having different horizontal and vertical scales. Vertical distortion was needed to accommodate the very large horizontal dimensions of the channels, yet ensure fully-turbulent flow, all within the aerial constraints of available laboratory space. Horizontal scales in excess of 1:1000 are not unusual. An important point is that the utility of vertical distortion diminishes for situations where two- and three-dimensional flow behavior strongly influence bed sediment movement. For these situations, typical of

complex channels such as the project site, vertical distortion must be kept to a minimum in order for the model to replicate sediment movement;

4. Many moveable-bed models used light-weight particles as model bed sediment. The range of particle-specific gravities is 1.05 (plastic) to 2.65 (quartz), with coal being about 1.25 to 1.50. With a submerged specific gravity[1] of 0.30, coal in water is just over five times as mobile as sand particle of the same diameter; plastic at 0.05 is 33 times as mobile. Franco (1978) suggests that coal has been the preferred modeling sediment for the USACE; 73% of the models he lists used crushed coal. Coal also is extensively used by other hydraulic laboratories (for example, Hecker et al. (1989) and Gabriel et al. (2007)). Unless the modeler, such as USACE, has access to a sizeable stockpile of model sediment, models of large channels normally use fine sand for model bed sediment. Use of sawdust, ground walnut shells, and plastic beads is largely limited to small models focused on the local flow field at a hydraulic structure such as a water diversion (e.g., Northwest Hydraulic Consultants Inc. (NHC 2012)). Useful discussions regarding the use of light-weight particles as model sediment are available from several sources; e.g., Gessler (1971), ASCE (2000), and Kocyigit et al. (2005);

5. Moveable-bed models often involve additional distortion in the form of slope distortion, also termed supplementary slope, in order to achieve adequate mobility of sediment movement in a model;

6. The literature contains several articles on moveable modeling involving braided-channel networks, though all except Klaassen (1990, 1992) describe models formed in laboratory flumes

[1] Submerged specific gravity $= (\rho_s - \rho)/\rho$, where ρ_s = sediment density and ρ = water density.

wider than about 8ft. Most laboratory models laterally constrain the development of braids, and thus are not models of braided-channel networks formed on wide alluvial plains. The studies reported by Zhu et al. (2010), Zhang et al. (2004), Warburton (1996), Davies and Lee (1988) and Ashmore (1982) describe hydraulic models or flume experiments used to investigate behavioral aspects braided-channel networks. Ashmore (1982), for example, describes a laboratory model typical of similar studies delving into braided-channel processes. Such studies commonly result in relationships between braided morphology, flow rate, bed sediment size, and channel slope. The comprehensive monograph edited by Sambrook Smith et al. (2006) says little about hydraulic modeling of braided channel networks, though is a useful overview of braided-channel processes. Klaassen (1990, 1992) describes modeling considerations associated with a large moveable-bed model used to ensure the reliable performance of a bridge across a wide braided channel. The model was constructed using a length scale L_r = 1,000 (Klaassen 1992), though it was originally described (Klaassen 1990) as being vertically distorted with a vertical length scale of 100. Klaassen's experience was initially followed in designing the present model, but it was found that his approach had to be significantly modified to better meet the purpose of the present model.

Considerations for the present hydraulic experiment, which involves the simulation of a braided-channel network formed on a wide alluvial plain, indicate that the model should use natural silica sand (not light-weight particles), because of the large volume of sand needed and the extensive handling of sand entailed in operating the model. Moreover, the model should not be considered vertically distorted, as Klaassen (1990) did for the model of the Jamuna River, because the model involves self-forming channels whose width to depth ratios should be comparable to those at the project site. The principal way to ensure adequate mobility of bed sediment in the present model will be to increase the model's slope relative to the longitudinal slope of the project site.

2.3 Remote Sensing and Photogrammetric Techniques

This thesis involves a review of literature on the collection of data associated with braided rivers via remote sensing techniques from both natural and laboratory settings. The review included the following sources: Ashmore et al. (2008), Ashmore et al. (2010), Bertoldi et al. (2006), Bezzola et al. (2006), Brogan et al. (2016), Casado et al. (2015), Chandler et al. (2002), Chipman et al. (2015), Dillabaugh et al. (2002), Gleason et al. (2015), Hicks et al. (2003), Lane et al. (2006). Some papers reviewed the basics of photogrammetric techniques. Many of the papers discuss the use of multispectral imagery in the field, and others where focus on the use of automated extraction of the data. Photogrammetric techniques were even used to decipher hydraulic parameters such as grain size, velocities and discharge. The photogrammetric and remotely sensed techniques presented in the above papers were examined for easy ways to determine a morphologic index that could be used to quantify the intensity of braiding throughout the experiment.

The following information was deduced from the review:

1. Multispectral data can be very useful in illuminating river morphology. Multispectral signatures can identify different substrates and materials. This method is extensively used in the field via satellite imagery, but less studied in laboratory settings. The cameras required to collect the necessary inputs for multispectral data analysis are very expensive;
2. The use of Digitally Elevation Maps (DEMs) are used in combination with photographic techniques to identify rivers from their surroundings;
3. The time to collect some data is longer than others and accuracy of image is highly dependent on the quality of the images produced;
4. Classification techniques can be very useful in the separation of data, but quality of the images used is highly dependent;

5. Programing for automated classification of photographs can be very time consuming and involve the use of expensive and advanced software;
6. RGB- oblique imagery data has been used for data collection of braided rivers and long-term classification studies; and,
7. There are many ways to quantify morphology using remotely sensed data. However, a channel count index is the preferred method because it is not sensitive to variations in channel sinuosity and orientation, has the smallest coefficient of variation, and can be measured quickly and reliably even from oblique imagery of a reach (Ashmore and Egozi 2008).

These considerations about remotely sensed data were used to select a suitable method of collecting the morphologic data needed for this study. The remotely sensed methods used in this experiment are discussed in Section 4.3.

3. Experiment Design, Construction, Calibration, and Instrumentation

3.1 Experiment Design

The flume layout used for the experiment originated as hydraulic model of a section of the North Fork Toutle River near Mount Saint Helens in the state of Washington. The dimensions and design of the experiment took into account the similitude considerations discussed in Section 2.2. The selection of parameters for the experiment involved an iterative process that began with selection of the experiment's length scale and sediment properties. The length scale was set to approximate 1/80 to the dimensions of the section of river chosen to replicate. The steps involved in designing the model required choosing a sufficient slope for the experiment, and then iteratively calibrating rates of sediment transport entering the model and the water discharge in order to produce a braided configuration similar to that of the project site.

Literature on mobile-bed modeling (e.g., ASCE 2000) and on braided-channel morphology (e.g., Sambrook-Smith et al. 2006, ASCE 2008) provide little quantitative guidance on the hydraulic relationships between water discharges, rate of sediment transport and bed slope associated with the formation of braided channels. Therefore, it was necessary to design the experiment based on an extensive period of calibration that evaluated the responsiveness to changes in water discharge and rate of sediment inflow. This calibration procedure required numerous repeated trials to arrive at a model bed reflective of the braided-channel network at the site, more about the final design parameters and the calibration can be seen in Section 3.5.

3.2 Layout

The experiment made use of CSU's 6.8m-wide, 29.2m-long, 1.0m-deep flume. Water flow through the open-loop system was driven by a 6HP centrifugal pump, which draws water from the sediment trap, then passes it along a 0.15m-diameter PVC pipe leading to a headbox that distributed flow into the model. A basic plan view of the model can be seen in Figure 2. The flume is also equipped with a motorized cart that can make the trip from upstream to downstream of the flume in approximately 3.2 minutes.

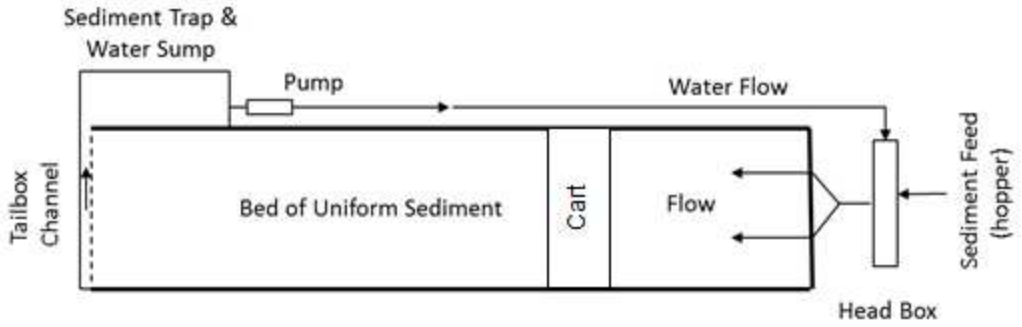

Figure 2: Plan view of the flume

The flume's layout can be seen in Figure 2, and incorporated the following features:

1. Water discharge, Q, passed through a closed-loop flow path, whereas sediment transport, G_s, occurred through an open-loop flow path via the upstream hopper;
2. Water recirculated through the model, being pumped from a purpose-built sump at the end of the model;
3. Sediment was fed into the headbox at a prescribed rate by means of a hopper that sat above a motor-driven auger, whose rate of rotation was adjusted to vary the rate of sediment feed in to the model;

4. The mix of water and sediment passed from the headbox entered a drop pipe connected to two identical, 6in-diameter pipes that discharged the mix into two starter channels that mimicked two main braids at the upstream end of the project site.
5. Sediment outflow from the model entered a steep-sloped trough at the downstream end of the model. Some sediment was conveyed with water flow along the trough to the sump, which served as a sediment trap. Sediment that collected in the trough (the sediment tended to accumulate as low dunes) had to be manually sluiced to the sump, as further explained in Section 3.5.

3.3 Experiment Construction

Figure 3(a)(b) shows the model under construction. Figure 4 shows the main components and dimensions of the model as constructed. The methods and materials used to construct the model are described below for the model's main components: the model bed, water-discharge flow path, sediment-transport flow path.

The bed was formed within the flume, whose walls are built from concrete blocks, and whose flat base is 0.35m above the floor of the laboratory housing the flume. The bed comprised uniform, 0.20mm-diameter silica sand, whose geometric standard deviation was 1.2, and specific gravity was 2.65. The bed's thickness varied from minimally 0.3m at the model's downstream, and thickened toward the model's upstream end. This thickness of bed was chosen so the model could accommodate for local scour.

An initial, longitudinal surface slope of 0.01 was used in forming the bed, and allowed to steepen to an average eventual slope of about 0.0135. The eventual slope extended from the invert of the exit of the

starter channel to the top of the sill at the downstream end of the flume. The bed was bounded at each upstream and downstream end by a 0.3m-wide, erosion-resistant sill formed of a mixture of pea-gravel and sand. The top elevation of each sill coincided with the top of the sand bed.

Water flow through the open-loop system was driven by a 6HP centrifugal pump, which drew water from the sediment trap, then passed it along a 6in.-diameter PVC pipe to the headbox. Water discharge to the headbox was controlled by means of a butterfly valve located downstream of an orifice plate used for flow metering. The headbox was a large (2.72m^3) steel-framed, steel-plate box into which the return flow entered, mixed with the sediment inflow, and drains through an 8in.-diameter PVC down pipe. This downpipe linked to two 0.15m-diameter PVC pipes, each of which issues water and sediment to a starter channel.

Figure 5a&b respectively depict the headbox and sediment mixing with water flow. The rate of sediment feed into the model was controlled using the auger and hopper arrangement. Two, short starter channels spaced 5.63ft either side of the flume centerline received water and sediment from the two pipes mentioned above, and discharged onto the model bed. To mitigate potential scour at the starter channels, the starter channels had a 0.3m-long brick base and were flanked by 2.5cm- to 5.0cm-diameter rock (Figure 6). Roughness elements were placed along the inside of the flume's sidewalls at the bed level so as to inhibit channel formation along the wall. These elements comprised concrete bricks spaced 5.0cm apart (Figure 7). The bricks sat on a metal rail fixed to the wall.

Flow exiting the model bed entered a steep tailbox channel whose invert sloped down (0.04 slope) towards the water sump and sediment trap shown in Figure 8. Sediment outflow from the model bed collected in the tailbox and was partially transported by flow through to the sump/sediment trap, where

the sediment collects. An adjustable chute at the end of the tailbox directed the sand to varying locations in the sump/sediment trap, keeping the area at the immediate downstream of the tailbox clear so that a collection cage could be placed in order to measure the rate of sand outflow from the model. The hopper above the auger was manually refilled with sediment as needed to keep the variance in hopper feed rate down. Sand accumulated in the sediment trap was removed manually on a several-day basis so that it did not affect the sump or accumulate enough to allow for recirculation of sediment.

(a) (b)

Figure 3(a)(b): Views of the model under construction (a) manual spreading of sand (b) placement of slope based guiderails along the flumes inner walls

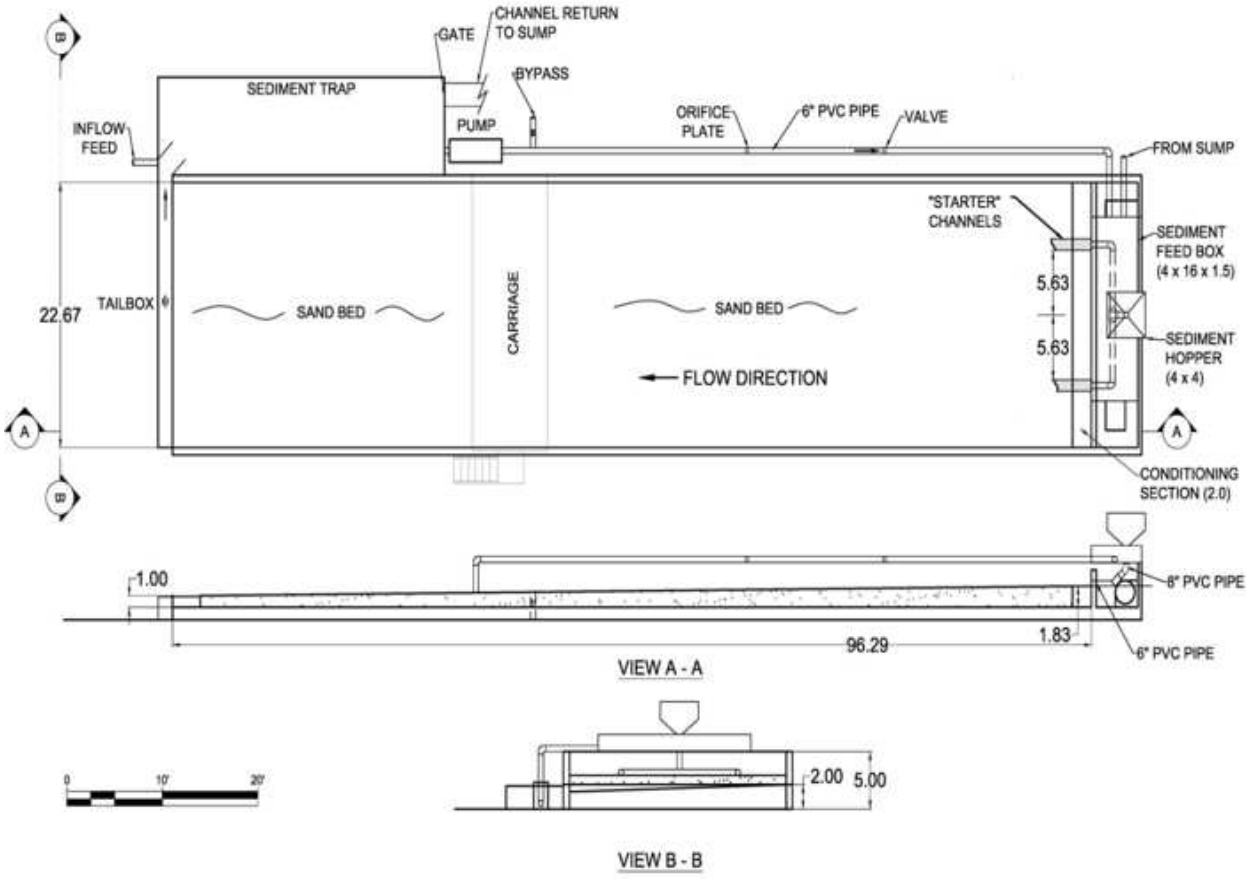

Figure 4: The main components and dimensions, shown in US customary units, of the model constructed in the flume

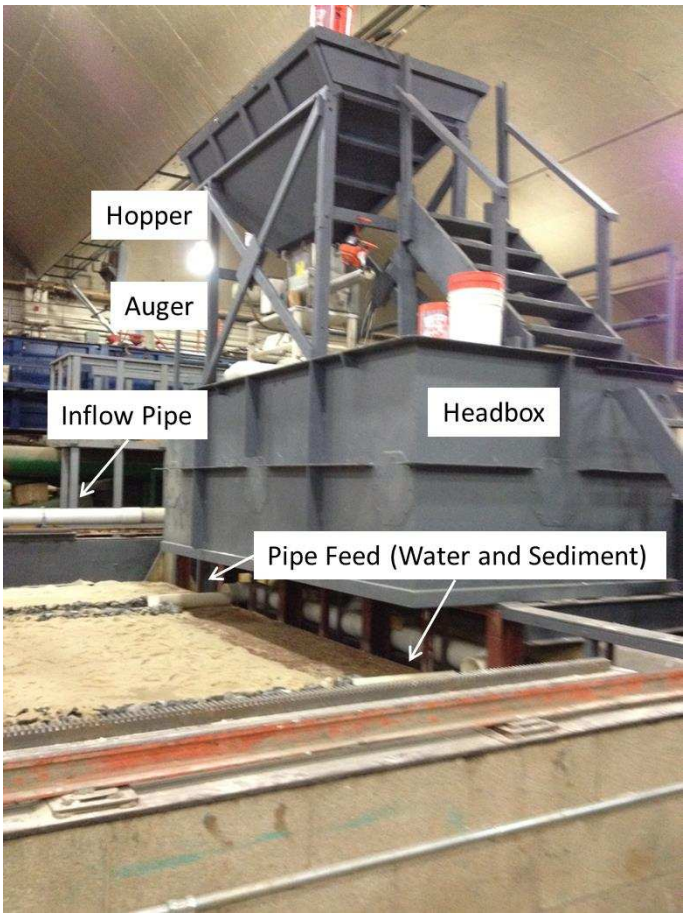

(a)

(b)

Figure 5(a)(b): Views of the headbox and hopper at the upstream end of the flume: (a) the hopper fed sediment via the auger into the headbox, whence water and sediment entered two pipes that discharged into two starter channels (braids); (b) a view of sediment mixing with water flow in the headbox

Figure 6: The two pipe-feed channels (simulating two main braids) issue water and sediment at the upstream end of the bed

Figure 7: Roughness elements (bricks) placed along the inside of each of the flume walls

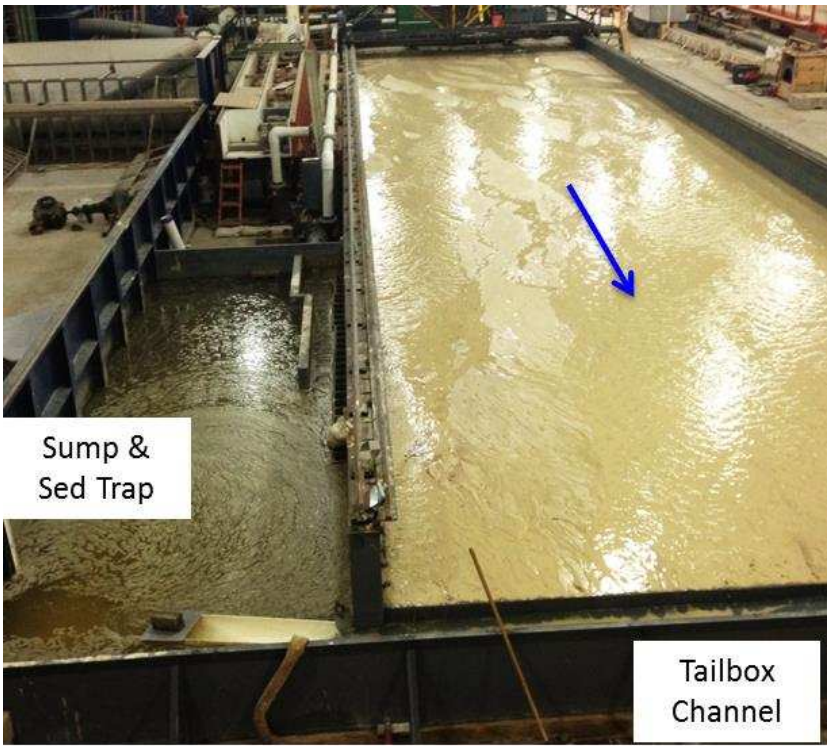

Figure 8: The tailbox channel, sediment trap, and water sump

3.4 Variables and Instrumentation

The experiment involved the following measured variables and instrumentation used to measure them:

1. Water discharge recirculated through the channel (closed-loop layout) was measured using a side-contraction orifice plate placed in the 0.15m-diameter pipe between the sediment trap and the headbox. A pressure transducer measured the head difference across the orifice plate and then a flow meter converted the head to a flow rate. The flow rate uncertainty obtained with the orifice plate was with 1% of the measured flow (per prior calibration test), and the resolution of the transducer was 3.0×10^{-4}m.
2. The rate of sand transport into the channel was measured by placing a $0.018m^3$ container beneath the outlet of the auger capturing sand outflow during a period of two minutes. The sand was then weighed so as to determine the mass rate of sediment inflow;

3. The rate of sand transport out of the braided channel was measured using a basket of 0.09m^2 cross-sectional area placed at the end of the tailbox channel for durations of one to five minutes depending on the magnitude of the rate of sediment outflow. The basket's dimensions were 0.3m by 0.3m by 0.6m high. When the basket was in position, a sliding plate along the tailbox skimmed sediment from the channel to the basket. After a period of time, ranging from 1-5 minutes depending on the outflow rate, the basket was removed. The depth of sediment in the basket was then measured after allowing the excess water to drain and the sand to dry. From there the volume and the mass rate of outflow calculated. Figure 9 (a) and (b) depict the sliding plate and basket placed at the end of the tailbox.
4. The surface topography and spatial coordination of the experiment were measured and recorded using a Leica Geosystems model HDS3600 LiDAR, with rated precision of 6mm at 50m.
5. Vibrant visualization of flow through the model was accomplished by means of the addition of fluorescent tracer dye that was diluted in the sump to the desired color. Dye injection enabled flow patterns to be observed and recorded more clearly at various locations in the model;
6. Water temperature was measured using a standard hand-held thermometer, and was approximately constant at 15^{o}C during the test series;
7. Morphologic observations and data was captured by two means. Time-lapse photography recorded by means of a Moultrie® Game Spy Plot Stalker 8.0MP camera placed at an elevated position with a useful overview of the model. Also, two digital Canon T3i Cameras with an 18-55mm lens, were used to capture high definition photographs along with exploring additional photogrammetric methods.

(a) (b)

Figure 9(a)(b): Measurement of sediment outflow from the model: (a) near the end of a measurement period, sediment was swept from the tailbox channel to the collection basket; (b) one of the two wire-mesh baskets used to measure the rate of sediment outflow from the model

3.5 Experiment Calibration

Calibration of the experiment involved two sets of activities, which explained in the following paragraphs:

1. Calibration of instrumentation such as flow meters, and instrumentation involved with sediment measurements.
2. Calibration of the water discharge, rate of sediment transport into the model, discharge, rate of sediment transport, and overall bed slope.

Calibration of the instrumentation was completed in preliminary experimental runs. This included examining variances in the sediment and water inflow along with optimizing the procedure for measuring the sediment outflow. Reported below is the instrumentation calibration procedures shown with their recorded variances, along with calibration procedures for the input parameters for the experiment.

The sediment inflow was controlled by a variable rate auger that could be set to different speeds. While a constant feed rate was used during testing there was slight variances in the output from the auger due to differences in water content and the amount of sediment that was in the hopper. To minimize the variance, it was determined that only sufficiently dry sand should be loaded into the hopper and it should be kept at least half loaded at all times. The recorded standard deviation for a sediment inflow value of 30.0 g/s was 2.65 g/s.

The water discharged into the model was controlled by a 6HP centrifugal pump that took water from the designed sump tank that was filled from an external water source. The flow was measured by means of an orifice plate that calculated flow through a pressure transducer that then output flow to a flow meter that read flow in terms of cubic feet per second. The flow was controlled by a butterfly valve and set to an averaged value of the flow meter readings, which had a standard deviation in its readings of 0.007. To minimize the variance in flow coming into the model the sump water level was kept at a constant level during testing.

The sediment outflow measurement procedure was calibrated based on maximizing the amount of sediment trapped each measurement. Due to the fine size of sediment, a screen size had to prove fine enough to trap all the sediment, and coarse enough so that water flow through the screen was not restricted. Several trap designs were examined in order to come up with the final design, which is shown in Section 3.4.

Calibration of the experiment involved the following sequence of steps leading to the experiment input parameters for sediment load, water discharge, and bed slope. The decision particularly considered the

influences of the following three independent parameters on two dependent parameters characterizing bed slope, *S*, and channel morphology (i.e., channel-braiding characteristics): i.e.,

$$S = \varphi_{Slope}\left(\frac{Q}{B\nu}, \frac{Q_S}{\rho Q}, \frac{Q_S}{B\sqrt{g(\Delta\rho/\rho)d^3}}\right) \quad \text{(Equation 1)}$$

and

$$Braiding = \varphi_{Braiding}\left(\frac{Q}{B\nu}, \frac{Q_S}{\rho Q}, \frac{Q_S}{B\sqrt{g(\Delta\rho/\rho)d^3}}\right) \quad \text{(Equation 2)}$$

It was useful to consider the similitude of channel dimensions as well as obtaining an overall braided morphology. Accordingly, a useful parameter is the ratio of main braid-channel width relative to flume width; i.e.,

$$W/B = \varphi'_{Braiding}\left(\frac{Q}{B\nu}, \frac{Q_S}{\rho Q}, \frac{Q_S}{B\sqrt{g(\Delta\rho/\rho)d^3}}\right) \quad \text{(Equation 3)}$$

Where: *ρ is density, d is depth, B is channel width, S is slope, Q is water discharge, Qs is sediment inflow, g is gravitational acceleration, v is kinematic viscosity of water.*

As ρ, $\Delta\rho$, *d* and *B* are constant for the experiment, calibration next entailed the practical step of expressing Equations 1, 2, and 3 in terms of working variables; i.e.,

G_S – mass (grams) of sediment per second entering the braided channel

Q – water discharge (m^3/s) through the channel

G_S/Q – concentration (g/m^3) of sediment in water entering the channel

Equations 2 and 3 can therefore be restated as

$$S = \varphi'_{Slope}(G_s, Q) \quad \text{(Equation 4)}$$

$$W/B = \varphi'_{braiding}(G_s, Q) \quad \text{(Equation 5)}$$

Several combinations of water discharge, sediment transport and slope could produce an equilibrium combination of S, G_S and Q; i.e., satisfy Equation 4, a sediment continuity check. However, a rather narrower set was needed to produce braiding geometrically similar to the braided channels at the project site; i.e., satisfy Equation 5, a braided morphology check.

The calibration steps followed from Equations 6 and 5, and required iterative adjustments of the three variables G_s, Q and S in order to produce a suitably braided-channel network:

1. The bed was set at an assumed initial slope, $S = S_0$, in a range likely to produce braided morphology, though channel dimensions were unknown. An initial bed slope for the model was selected as $S_0 = 0.01$;
2. Two pre-formed main braid channels were set at the upstream end of the model. Each channel supplied equal inflows of sediment and water to the model;
3. An approximate initial value of Q was estimated based Froude Number similitude;
4. An initial value of G_S was selected based on G_S/Q values used in prior studies of braided channels. A magnitude of bed sediment transport was chosen using values of G_s/Q from prior hydraulic models of braided channels. The calibration tests increased G_s from about 5g/s, 25 g/s to 50g/s for a model value of water discharge equivalent to a prototype discharge of 170m^3/s;
5. The initial values of S_0 and G_S and Q were checked to determine if the temporal average rate of sediment transport out of the flume equaled the steady rate of sediment inflow into the flume (*sediment continuity check*);
6. The initial values of S_0 and G_S and Q were also checked to ensure they produced a braided channel network in the model, and that the network was reasonably similar – notably, that W/B was adequately similar to that observed at the site during full-scale water discharges of about 6,000cfs or thereabouts (*channel morphology check*);

7. If sediment continuity did not occur, the initial value of Q was slightly increased and steps 5) and 6) were repeated over a period of time (one to two days);
8. Step 7) was repeated with an adjustment to G_S. This step was hastened by jointly adjusting Q and G_S, and letting S adjust in response, so as to produce a braided-channel network;
9. When the channel morphology of the braided network (notably, values of W/B) compared well with that observed at the site, S was left to adjust to an equilibrium final value of 0.0135; and,
10. The finalized values of G_S, Q and S prescribed the key baseline information needed to operate the experiment.

The final values used in the experimental procedures are described in full in Section 3.6.

3.6 General Procedure

Prior to initiating the experiment, extensive calibration runs were completed to determine input parameter values that allows the flume to reach a sustainable dynamic braided configuration. The final input parameters used in the experiment are as follows:

1. Bed Slope = 0.0135
2. Sediment Inflow = 30 g/s
3. Water Inflow = 0.00396 m^3/s

Before the experiment began, the bed of the flume was smoothed to a plane bed surface that matched the designed valley slope, 0.0135. An example of the smoothed flume bed surface is illustrated in Figure 10. LiDAR surveying was used to check the relative lateral levelness and slope of the flume bed before water was ran over the surface. A slight berm was added to each side of the flume to promote braided channel establishment in the middle of the flume rather than along the walls. After the flume was leveled, preliminary runs were completed using the prescribed input rates to allow channels to develop

and to ensure equilibrium before the experiment began. Due to the channels being self-forming, substantial time (about 30 hours) was required for the flume to reach relative equilibrium.

Figure 10: Leveled flume bed before testing

Equilibrium of the experiment was determined from the plot of accumulated sediment inflow compared to the relative slope of the accumulated sediment outflow plot. An example of obtaining equilibrium during the calibration runs using the prescribed parameters can be seen in Figure 11. In the figure the dotted line is shown to parallel that of the cumulative sediment inflow value. When the cumulative sediment outflow value approximately paralleled the cumulative sediment inflow value, equilibrium was assumed and the experiment began.

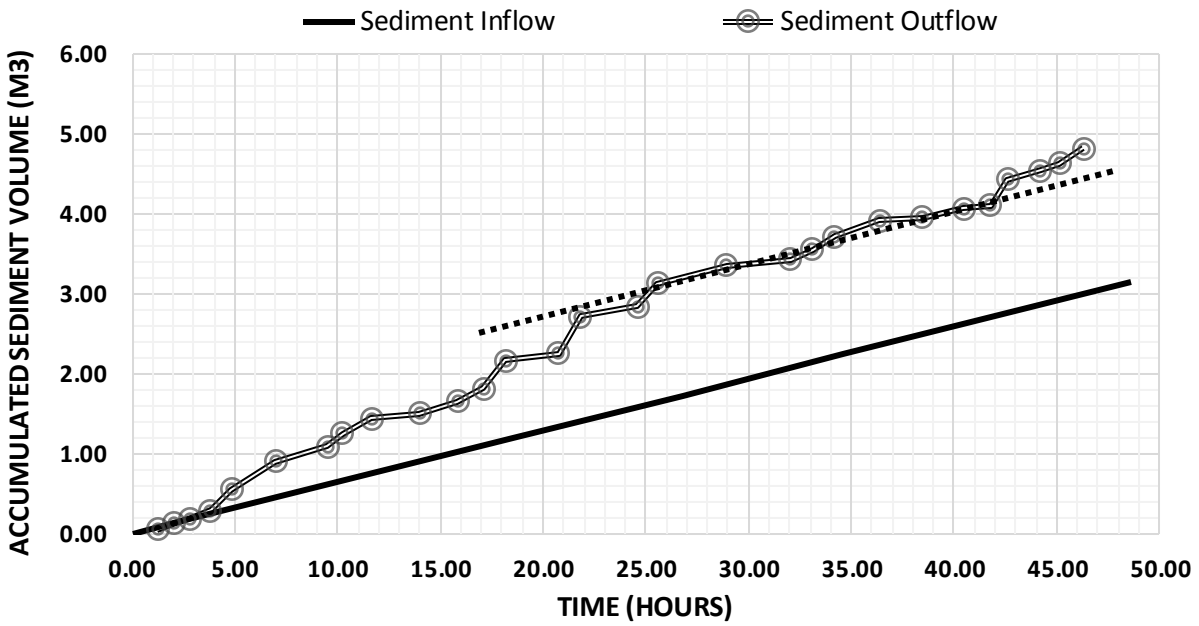

Figure 11: Cumulative plots of sediment inflow and sediment outflow shown to demonstrate equilibrium, the dotted line is shown to parallel the sediment inflow plot.

Once equilibrium had been established, the experiment ran continuously except, due to safety constraints, it was not run overnight and had to shut off between data-collection days. The experiment was started the next time by easing into the prescribed input values so not to cause unwanted erosion of the established channels. During the experiment, strict timing of data collection was imposed so that a comprehensive data set could be obtained. Sediment outflow measurements were obtained at least once an hour, while morphologic measurements needed to coincide with the timing of the sediment measurements. The input parameters were also checked regularly to ensure prescribed rates. Other maintenance and flume upkeep was also necessary during experimentation to ensure the sustainability of the experiment.

4. Data Collection

4.1 Hydraulic Data Collection

The main hydraulic parameters measured throughout the study were the rate of water flow, and the rates of sediment inflow and outflow from the model. There was extensive calibration of the methods used to collect and monitor these parameters. Further explanation of the calibration of these can be found in Chapter 3. The rates of sediment and water inflow were measured periodically throughout the testing to ensure they stayed at the prescribed rates. The water level in the sump was maintained at a constant level to ensure these parameters remained steady during the experiment. Additionally, the sediment hopper was kept stocked with sieved sand. Sediment outflow data were collected approximately every hour to ensure a comprehensive data set was obtained.

The collection of the sediment outflow process is explained here. Shown in Figure 12 the bed sediment is transported downstream and out of the flume by the water flow through the flume. The water sediment mixture then enters the steep chute that conveys the flow into the sediment trap and sump area to the side of the flume. When a sediment outflow measurement was to be made, the chute was swept clean of all sediment and the sediment measurement basket was placed under the end of the chute, which was designed to fit the basket securely, and a timer was started. During the collection process, the chute was continuously swept, demonstrated in Figure 13, to help convey the sediment into the basket for a period of 2-10 minutes depending on the intensity of the sediment outflow during the measurement. With a final sweep of material from the chute to the basket, the basket was removed and rinsed to allow for all the collected sediment to be leveled on the bottom of the basket. The sand was allowed to dry to remove excess sediment before a 9x9 grid depth sampling method was used to get an averaged depth of sediment accumulation. The depth measurement was then converted (taking

into account accumulation void ratio) into a volume of sediment outflow, from which volumetric and mass rates of sediment outflow were calculated. Chapter 4.2 elaborates this procedure.

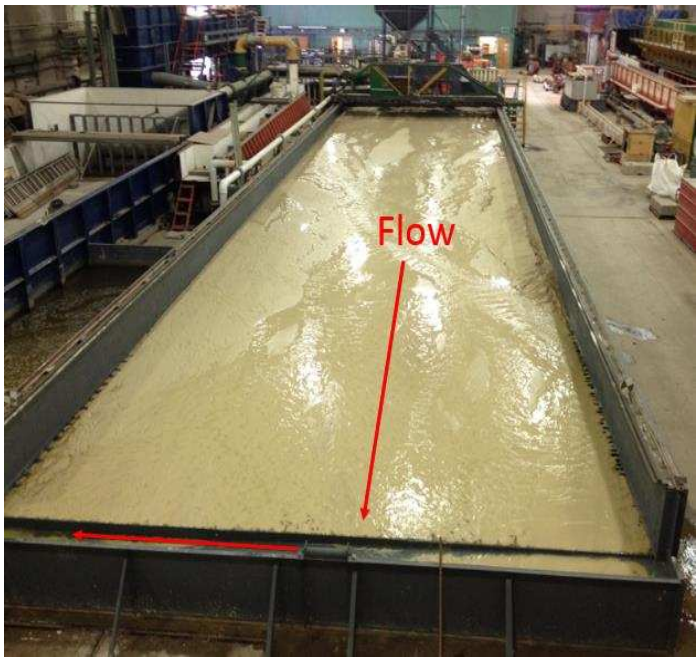

Figure 12: Sediment transport path through the flume and down the outflow chute highlighted

Figure 13: Sediment collection "chute sweeping" process shown

4.2 Hydraulic Data Analyses

To analyze the data, a strict record of time was kept so that all the measurements would coincide with the length of time the model was running. Microsoft Excel was used to document all hydraulic testing records to analyze the data for variation and for plotting figures. The conversion of sediment outflow rate from volumetric rate was based on using a porosity of 0.36 (determined from an auxiliary test) and the calculations from a volumetric rate to a mass rate are as follow.

$$p_0 = \frac{\forall_v}{\forall_t} = 0.36 \qquad \text{(Equation 6)}$$

Where: p_0 is porosity,

$\forall_v$ is the volume of void space, and

$\forall_t$ is the total volume.

The porosity is then used to calculate the dry density of the mixture, defined as the mass of solid per unit total volume, as follows:

$$\rho_{md} = \frac{M_s}{\forall_t} = \rho_s(1 - p_0) = 2650\,\frac{kg}{m^3}(1 - 0.36) = 1{,}673\,\frac{kg}{m^3} \qquad \text{(Equation 7)}$$

Where: ρ_{md} is the dry specific mass of the mixture

M_s is the mass of the solid,

$\forall_t$ is the total volume,

ρ_s is mass density of solid particles, 2,650 kg/m^3 for quartz sand, and

p_0 is porosity.

So then, it follows that for all conversions from a mass rate to a volumetric rate, and vice versa, dry specific mass value of 1,673 kg/m^3 was used, which accounts for a sediment-accumulation porosity of 0.36. Also for all volumes were recorded as a total volume, including both the voids and the solids of the

mixture. In summary, the mass rate of sediment outflow was estimated using the conversion (volume of sediment accumulated in the basket)x(1,673kg/m^3).

4.3 Morphologic Data Collection

There were two main goals in using photographic methods to collect morphologic data.

1. Quantify the intensity of braiding in the model in terms of a morphologic index.
2. Track morphologic changes in the model and identify modes of braided evolution.

The braided morphologic index first used for the experiments was based of the anabranch channel count index (channel count index) which was a method recommended by Ashmore and Egozi (2008). This method was relatively easy to implement, even when using oblique photographs of the braided channel. In order to accurately measure the channel count index, imagery needed to capture the full extent of the braided reach and equidistant cross sections had to be established in the photographs. The channel count index involved counting the main anabranches at defined cross sections along the braided channel. Once the channel count index has been determined for all cross sections in the reach, the index is averaged to find the resulting channel count index. In order to accuracy asses the channel count index it is recommended that the number of cross sections in a reach must exceed 10 and they must be spaced no closer than the average wetted width of the channels (Ashmore and Egozi 2008). It was found that the variability in the braided index was minimized when a reach was divided into 11 cross sections or more, (Ashmore and Egozi 2008).

To record the channel count index, and to gain an understanding of the chronological progression of sand accumulations in the model, three photographic methods were tested for use in this experiment. The methods tested are an aerial panoramic approach, structure for motion photography, and an

oblique photographic approach. With these photographic approaches several criteria were examined to determine the method that would be most effective for use in this study:

1. Ability to capture entire flume within a relatively short amount of time due to the rapidly shifting morphology;
2. Processing time;
3. Clearness of the inundated areas vs non inundated areas; and,
4. Overall simplicity of application.

4.3.1 **Aerial Imagery-**

Due to the large width of the flume, two cameras were needed to capture the full flume from an aerial angle. The two cameras where mounted on the cart to a height that was optimized for accessibility and field of view. Figure 14 shows a plan view approximation of the camera setup and capture range. Each camera was able to capture about 70% the width of the flume, while being able to capture about 12 feet of the flume longitudinally. Photographs from each camera were taken at 5 foot intervals going down the length of the flume. This procedure gave significant overlap in the views captured by the photographs and enabled the photos to be merged. A bubble level on the camera mount was used to ensure that the cameras were mounted on a level seating. In total, 17 photographs from each camera were needed to traverse from top to bottom of the flume. Therefore 34 photographs were taken per procedure, which took on average about 5 minutes. The cart was stopped at each interval to ensure each photograph was not blurred.

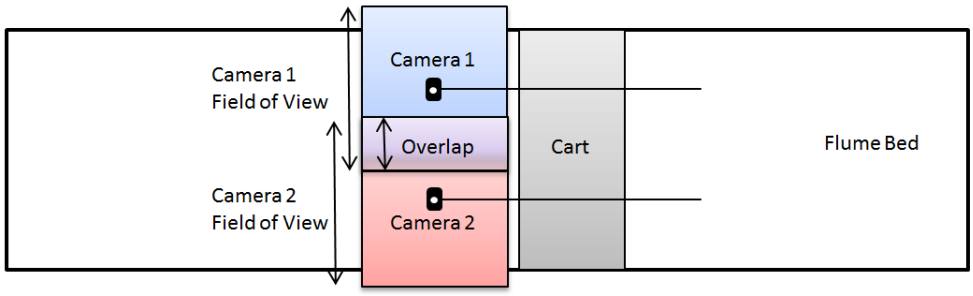

Figure 14: Plan view showing approximate location and field of view used in the aerial imagery

After the photographs were taken, panoramic imaging software was used to stich the photos together without the use of ground control points. Several software programs for photograph–stitching were compared to decide which one was the best option to use. These programs included: Adobe PhotoShop, GIMP 2.0, AutoStitch, and Microsoft Image Composite Editor. The best program for this study was Microsoft Image Composite Editor, due to its ease of use and the overall quality of the image it produced. An example stitched image can be seen below in Figure 15.

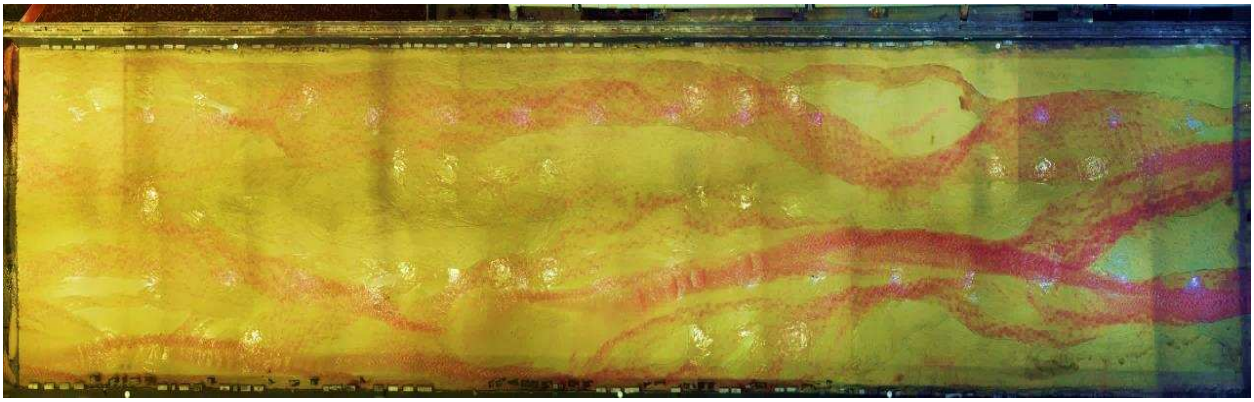

Figure 15: Aerial panoramic image of the flume; flow is to the readers left

Additional post processing of the resulting aerial image of the braided channel included contrast and brightness adjustments and the development of cross sections. Contrast and brightness adjustments

were made to increase the visual separation between the inundated versus the non-inundated areas. The cross sections were developed based on pixel location in the image, and digitized into the image via MATLAB 2015b. Figure 16 shows a resulting image.

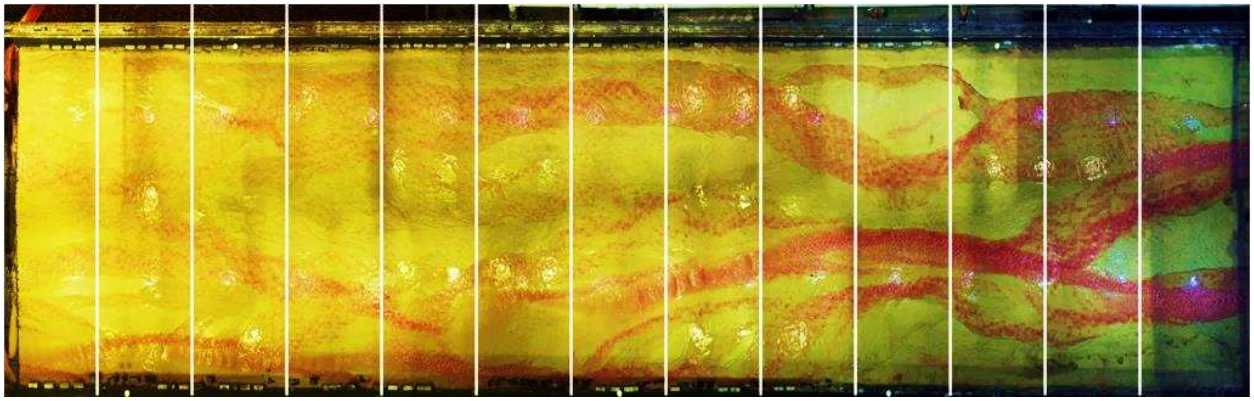

Figure 16: Aerial imagery shown with projected cross sections; flow is to the reader's left

4.3.2 **Structure from Motion Photography-**

Structure-from-motion photogrammetry uses multi-view computer vision methods that detect and match features between images in order to estimate the three-dimensional structure and camera locations and angles simultaneously (Morgan et al, 2016). This method has little recorded use in the laboratory setting, but is becoming increasingly popular in field applications. It uses multiple photos of the same object to create a three-dimensional point cloud, and has ortho-rectification capabilities. Although there are several programs that offer structure for motion capabilities, Agisoft PhotoScan Professional was used for this study. The cart was constantly moving while approximately 50 photos were taken in the downstream direction. This procedure produced a sufficiently dense point-cloud to create the final ortho-rectified image. One camera was mounted on the center of the top of the cart. The camera captured the flume at an oblique angle approximately 40° to the horizontal so that both

sides of the flume were seen in the image. A plan view of the structure from motion photogrammetry set up is shown in Figure 17, and an example resulting ortho-rectified image is shown in Figure 18.

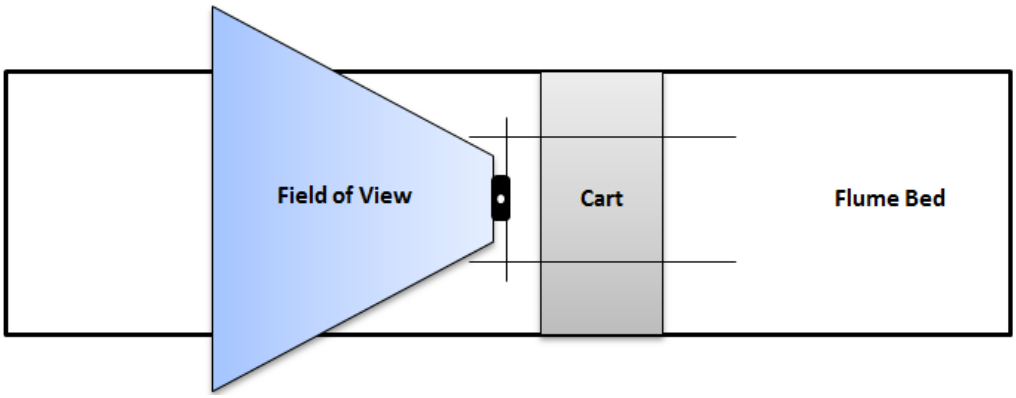

Figure 17: Plan view of the structure from motion photography set up

Figure 18: Structure from motion ortho-rectified image; flow is to the reader's left

Additional post-processing of the aerial image included contrast and brightness adjustments and the development of cross sections. The contrast and brightness adjustments were made to increase to contrast between of the inundated vs the non-inundated areas. The cross sections were then developed

based on pixel location in the image and digitized into the image via MATLAB 2015b. An example view can be seen in Figure 19.

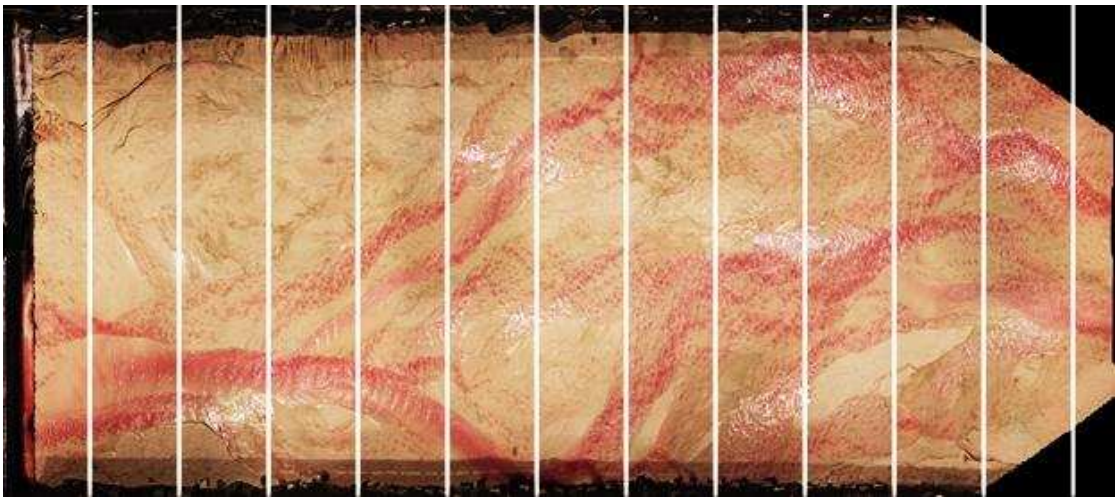

Figure 19: Structure from motion photography shown with the digitized cross sections, contrast and brightness edits; the flow is to the reader's left

It should be noted that this method was attempted several times with no success. It was only when the laboratory received new LED lighting that an ortho-rectified image from structure from motion was produced. The method is highly dependent on the photographic technique, including the overall lighting, and quality of the images used.

4.3.3 **Oblique imagery-**

The oblique imagery method used an 8 megapixel camera mounted directly in line with the flume. The camera's angle enabled the entire flume to be captured in a single photograph. This advantage was increased, because images could be taken every 15 minutes during the experiment. The location of the time-lapse camera can be seen in Figure 20, and an example unprocessed time-lapse photograph of the flume is shown in Figure 21.

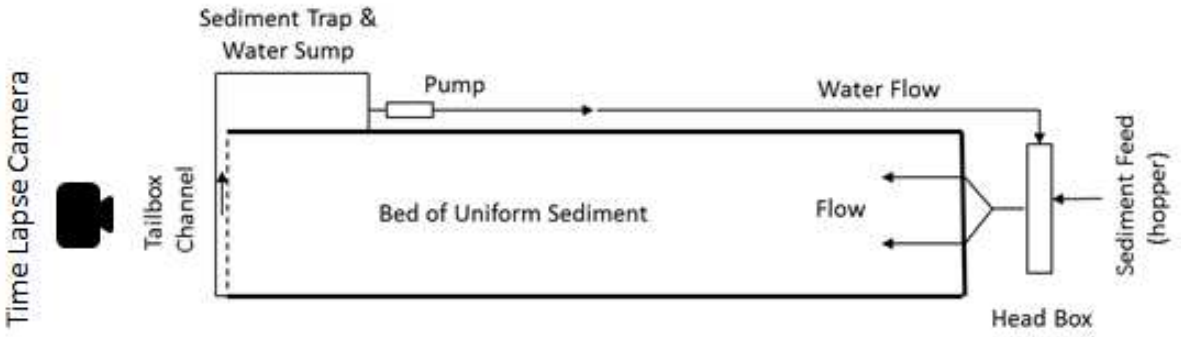

Figure 20: Plan view of the location of the oblique angled time-lapse camera

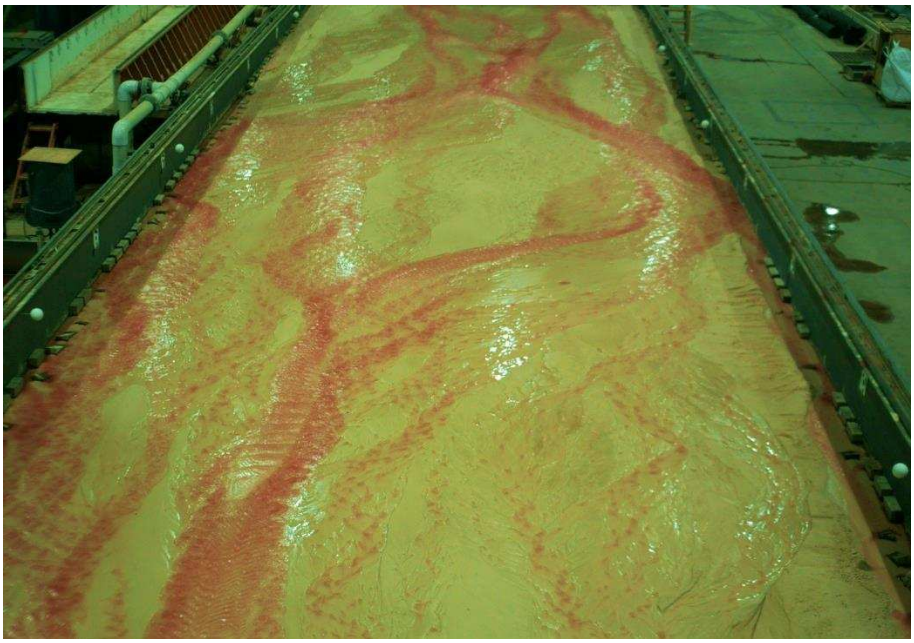

Figure 21: An unprocessed oblique photograph of the flume captured by the time-lapse camera; flow is from top to bottom

Post-processing included optimizing contrast and brightness settings along with establishing equally spaced cross sections. Creating cross sections on the oblique image was completed with the aid of LiDAR and image pixel location. Target locations were collected via LiDAR and compared to the pixel locations of the targets in the photographs. A polynomial equation was then developed that allowed for equidistant cross sections to be developed in relation to the skew of the photograph . Once the location

of the cross sections was determined, MATLAB 2015b was used to digitize the cross sections onto all the photos. The final oblique image product used for analysis is shown below in Figure 22.

Figure 22: A time-lapse oblique photograph shown with the overlaid cross sections, and with contrast and brightness corrections; flow is from top to bottom

4.4 Morphologic Analysis

The photographic method that proved best suited for the experiment was the oblique time-lapse imagery method. This method allowed for an automated and timely collection process that also produced the least spatially altered image. In addition, due to the angle of the images and different reflective properties of water and sand there was a clear separation of inundated and non-inundated areas. The visual separation occurred even without the addition of tracer dye as shown in Figure 23.

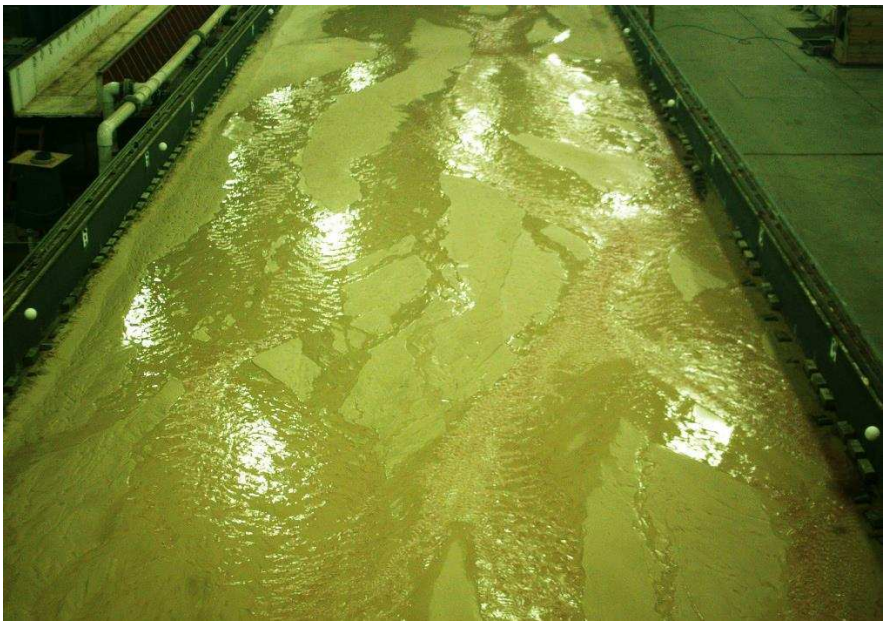

Figure 23: This oblique photograph with no tracer dye shows that the anabranch boundaries could be well defined; the flow is from top to bottom

When analyzing the photos taken using the channel count index, it was noted that the method was not scientifically sound for use in this study. This was due to the occurrence of intermittent sheet flow that was observed during testing. In other words, issues arose when there was a very wide inundated section that had multiple shallow channel paths crossing through with overbank flows that connected them all. This issue led to inaccuracies in the channel count index method. Figure 24 shows an example of when this method did not accurately assess the true morphology of the model. As seen at the bottom right of the figure there is a sheet flow that contains multiple channels. The shallow nature of these channels made them hard to detect viewing through water. This difficulty was problematic for the morphologic analysis. For example, with the channel count index a large sheet flow could count only as one anabranch; a sheet flow typically indicated a depositional plain, whereas a true large anabranch typically indicated increased aggradation and a high flow of sediment.

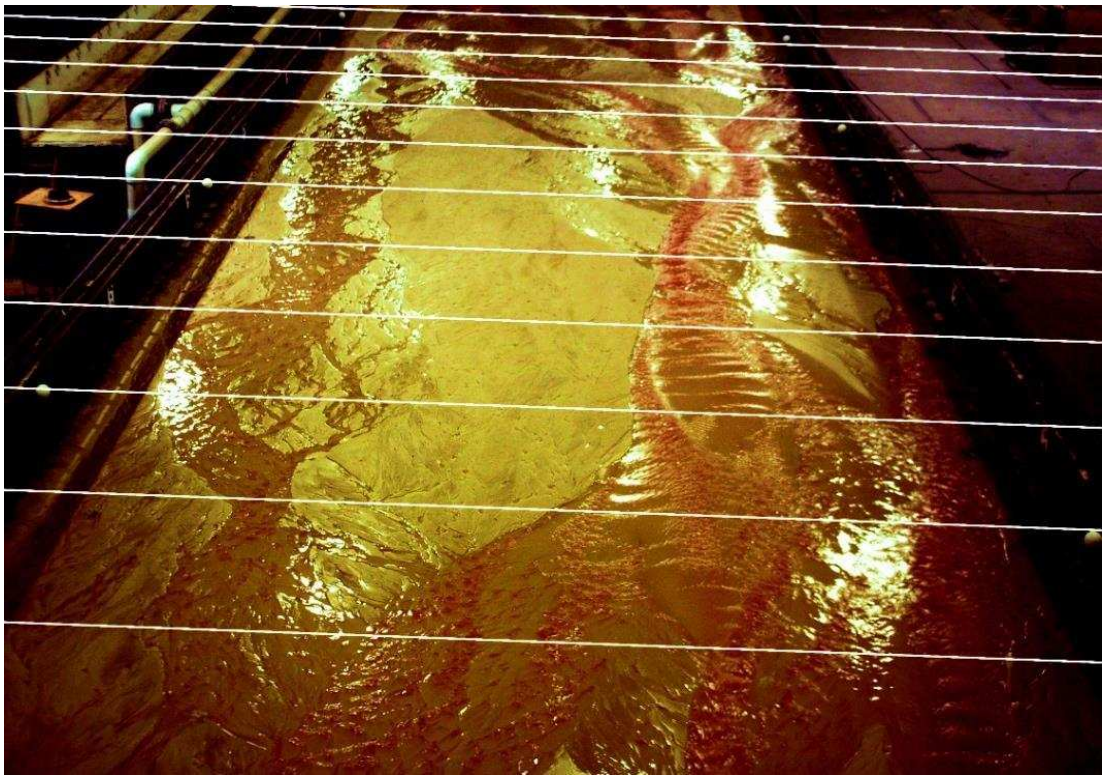

Figure 24: Inaccurate channel count index due to sheet flow near end of model containing multiple channels; the flow is from top to bottom

Therefore, a new way to characterize and quantify the morphology of the braided channel had to be established. Keeping the channel count index in mind, the same cross sections were used. The new morphologic parameter was termed the "*Flow Width Ratio,*" or FWR, and is defined as the total width of water flow across a cross section of the braided channel divided by the full width of the braided channel. FWR has a value of one being the highest value of measured braided intensity, and a value of zero being the lowest. While this method for measuring braided intensity seems to have not been used in prior studies it proved to be a more accurate, scientific, and repeatable procedure for the present experiment.

It is important to note that the present experiment was ran at a constant discharge and the FWR should not be used to evaluate unsteady flow conditions. The method was designed to closely emulate the

channel count index with the added ability of more accurately quantifying the sheet flows witnessed. A temporal comparison of the methods is shown in Figure 25 and a regression of the two methods is shown in Figure 26.

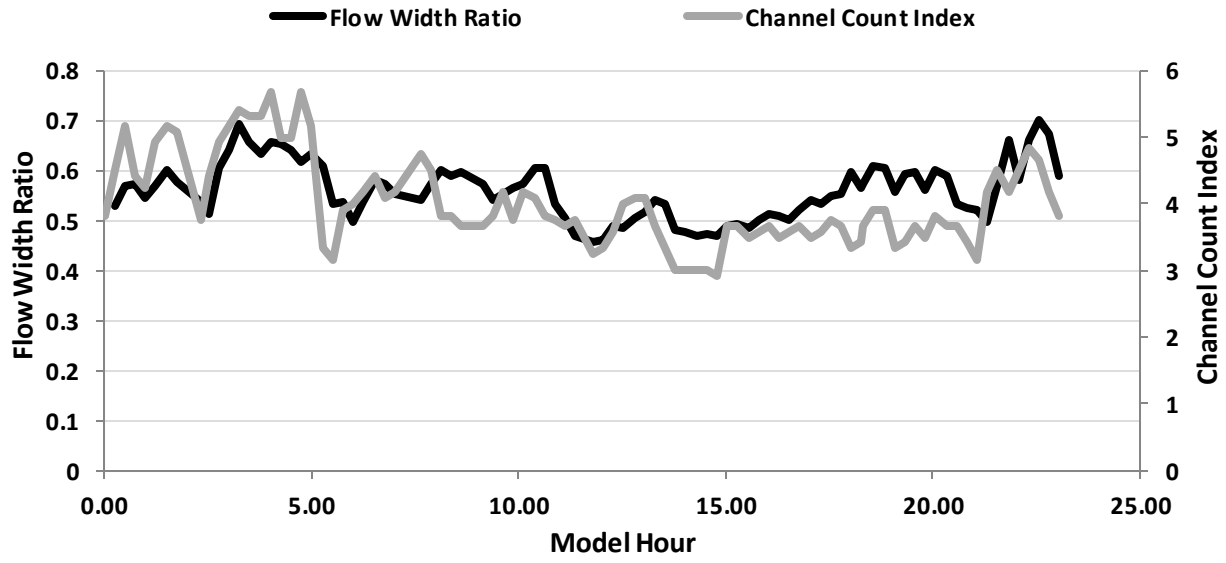

Figure 25: Temporal plot of the channel count index versus the flow width ratio

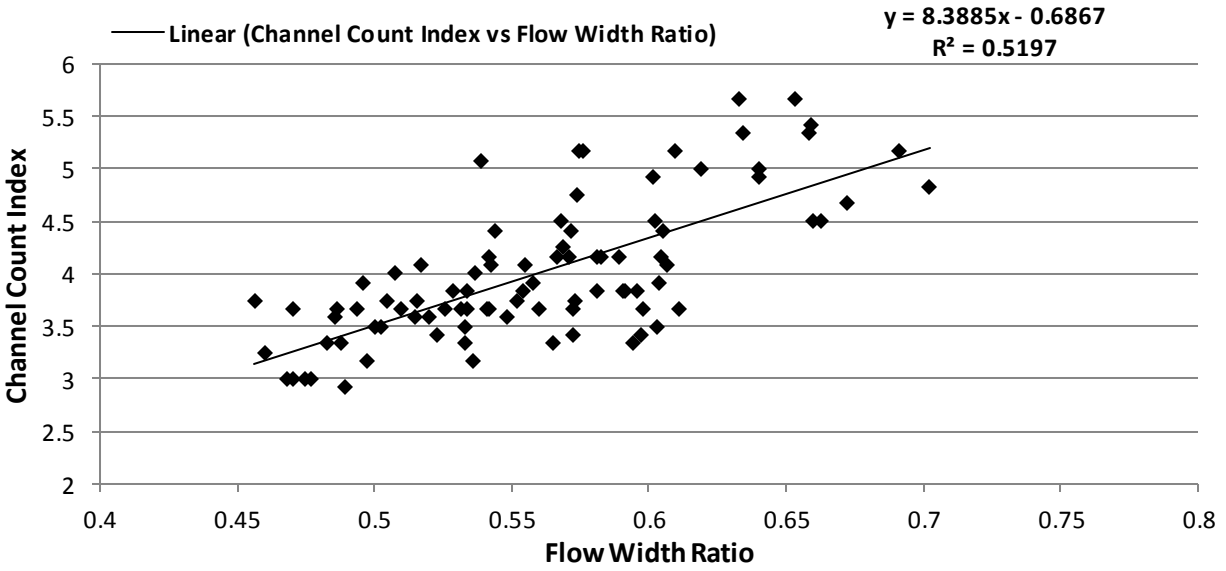

Figure 26: Linear regression of the channel count index versus the flow width ratio

Figure 26 shows there is significant agreement between measuring the braided intensity using the well-studied channel count index and the new method of the flow width ratio. Therefore, for the purpose of this experiment and paper, the flow width ratio was used to measure braided intensity in the channel. Using the photographs and the FWR method, each cross sectional braided intensity was analyzed and then averaged over the reach to determine the overall value. This method allowed for all the widths of the anabranches and the widths of the flume at each cross section to measured accurately using a pixel count measurement in the image analysis tool included in the MATLAB programming software. Figure 27 below shows the same image as Figure 24, but with measurements taken via the MATLAB image analysis tool shown for all individual anabranches.

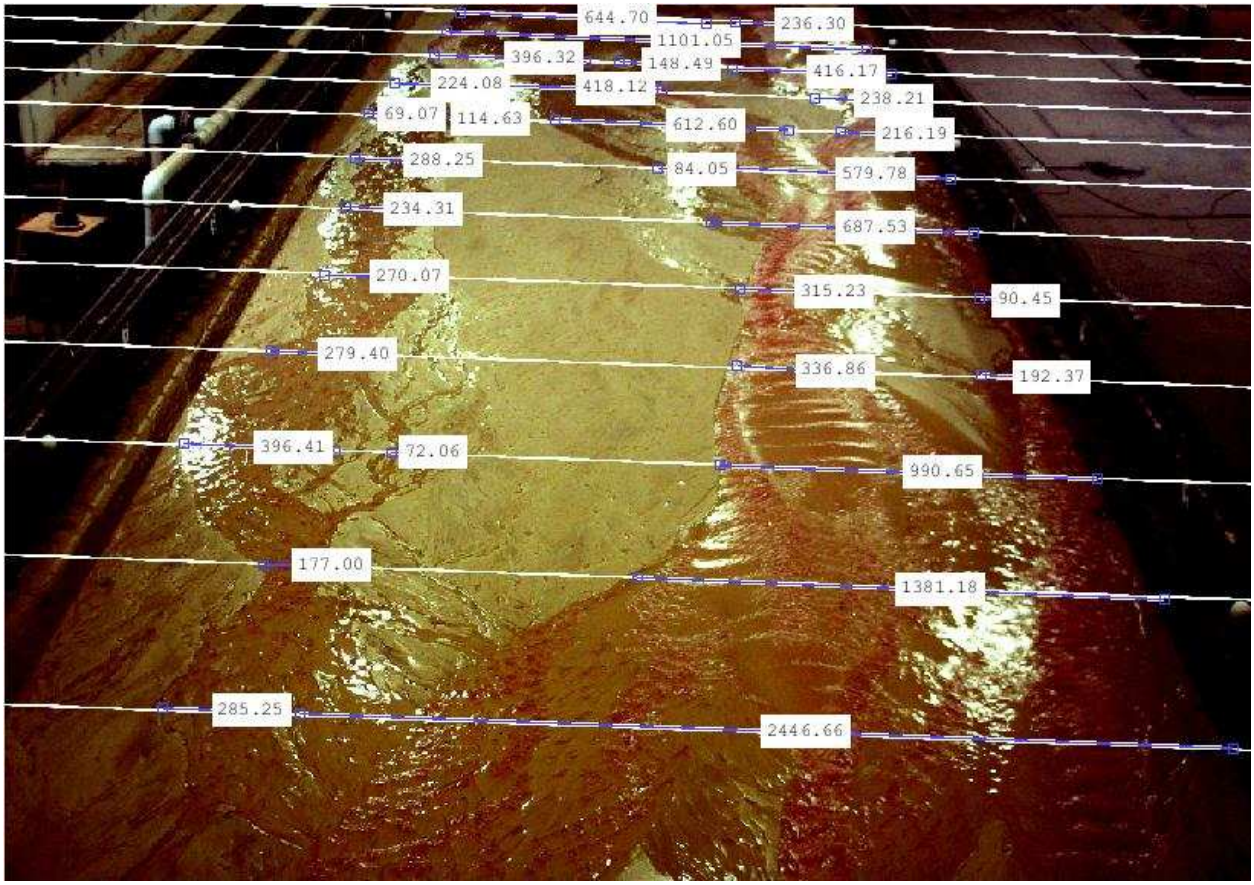

Figure 27: Width measurements taken with MATLAB image tool for all existing anabranches shown, flow is from top to bottom.

5. Results

5.1 Introduction

The results of the testing are divided into two separate sets of data, each set consisting of approximately 40 hours of data measurements. The two sets are distinguished by the labels Run 1 and Run 2, with Run 1 being the first set of testing and Run 2 being the second. Ideally, there would be one solid set of data however, towards the end of the first set of data the braided channel was preferentially flowing to one side of the flume and the dynamic shifting of the braids previously witnessed had halted. This study focused on the dynamic behavior of braided rivers, and because the model was experiencing a period of minimized dynamic behavior due to elevated degradation along the wall the decision was made to re-establish the model to show more dynamic morphologic behavior without the added affects from the wall. If the test continued, the flume may have eventually changed its path. However, for the purpose of this experiment and because of time constraints the model was re-leveled and ran for a period to allow an adequate equilibrium braided channel to re-establish within the limits of the walls of the flume. There are two things to note from this occurrence that can be related to natural systems:

1. Rivers follow the path of least resistance which in this case was the smooth wall of the flume
2. If laterally unconfined the braided belt would have continued to shift which could not have been witnessed by the confined space of this experiment.

The present chapter comprise three sections of analysis. The first section considers the results from the sediment-transport data collected during testing. The second section examines the morphologic data collected during testing, which consist of measured data and observed data. The third section compares the sediment data and the morphologic data. Each section contains an introduction presenting the data and a discussion of the data presented.

5.2 Sediment Outflow Data

The sediment outflow data shown consist of sediment transport and cumulative sediment transport data plots. The plots of cumulative sediment transport also show the accumulation of sediment in or out of the model and provide a better picture of what state the model was in during testing; i.e., aggradation, degradation, or equilibrium. Aggradation in the model indicates a higher rate of sediment inflow accumulation than accumulated outflow of sediment. Degradation in the model indicates a higher accumulated amount of sediment outflow than sediment inflow. Equilibrium in the model indicates an equal amount of accumulation in sediment outflow and sediment inflow. While the model was in relative equilibrium throughout the testing, each sedimentary state existed periodically throughout the experiment.

The sediment outflow was measured approximately once per hour and the sediment inflow was measured periodically. The measurements of sediment inflow fluctuated slightly, but averaged the designated value of 30 g/s. The accumulation of the sediment flow was calculated based on an average of the two adjacent measurements. The sediment outflow rate plots show the sediment out flow rate plotted with the averaged prescribed sediment inflow rate. The sediment inflow rate shows the assumed value of equilibrium in sediment transport through the model. Plotting the inflow and outflow rates of sediment transport usefully portrays the dynamic nature of sediment transport through the flume.

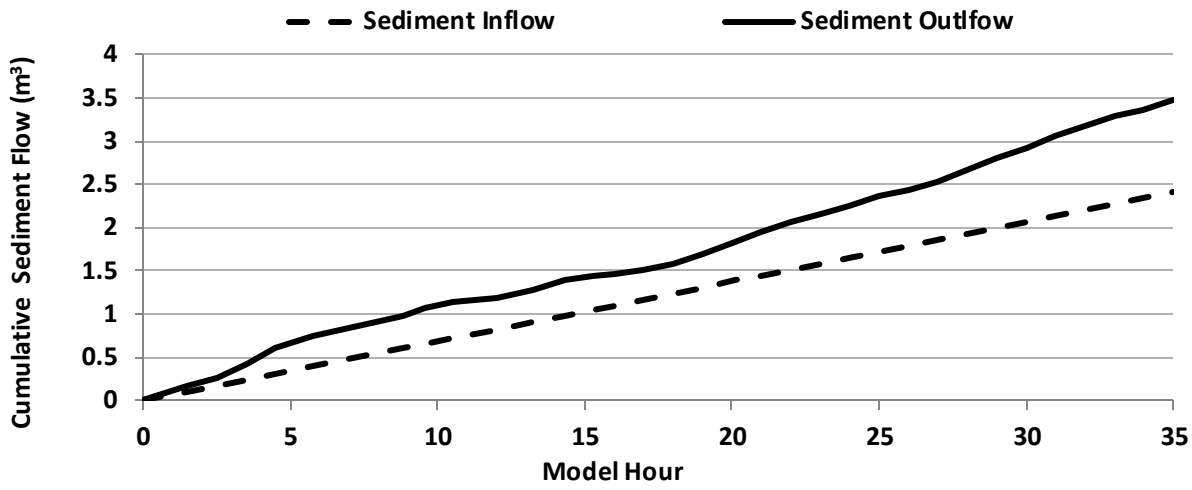

Figure 28: Run 1 cumulative sediment inflow and sediment outflow plot

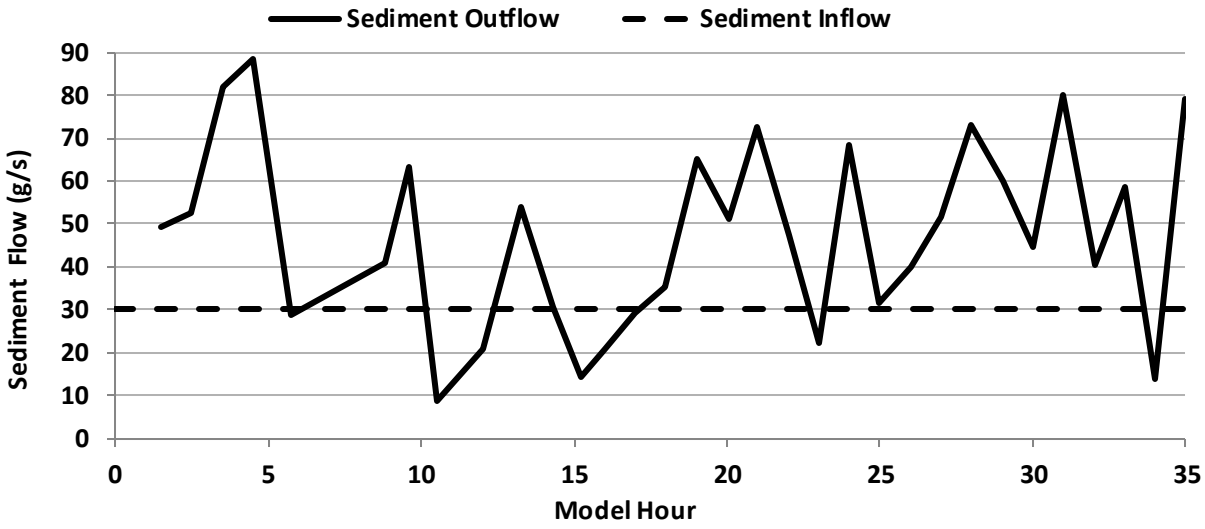

Figure 29: Run 1 sediment outflow measurements and averaged sediment inflow shown

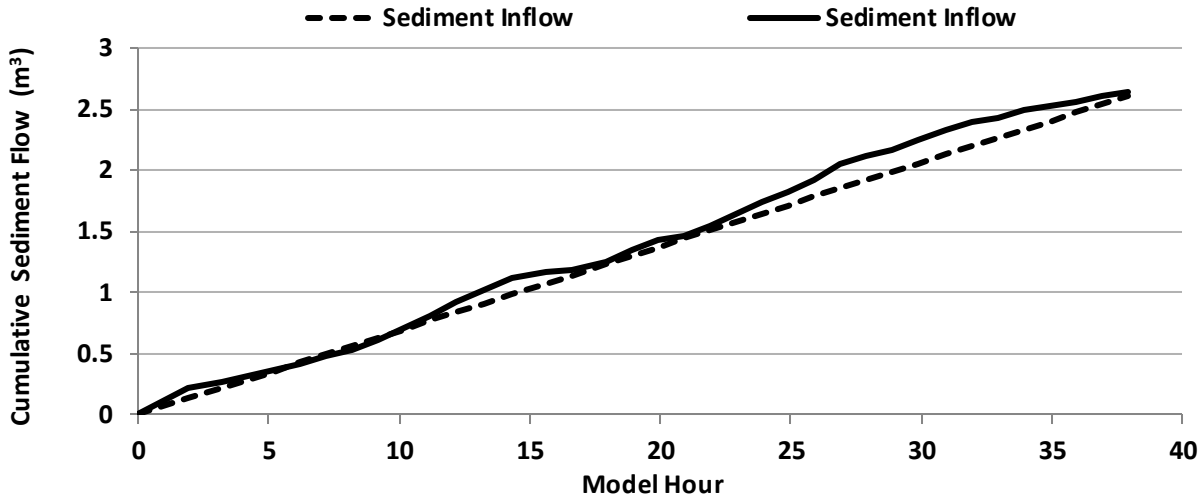

Figure 30: Run 2 cumulative sediment inflow and averaged sediment outflow plot

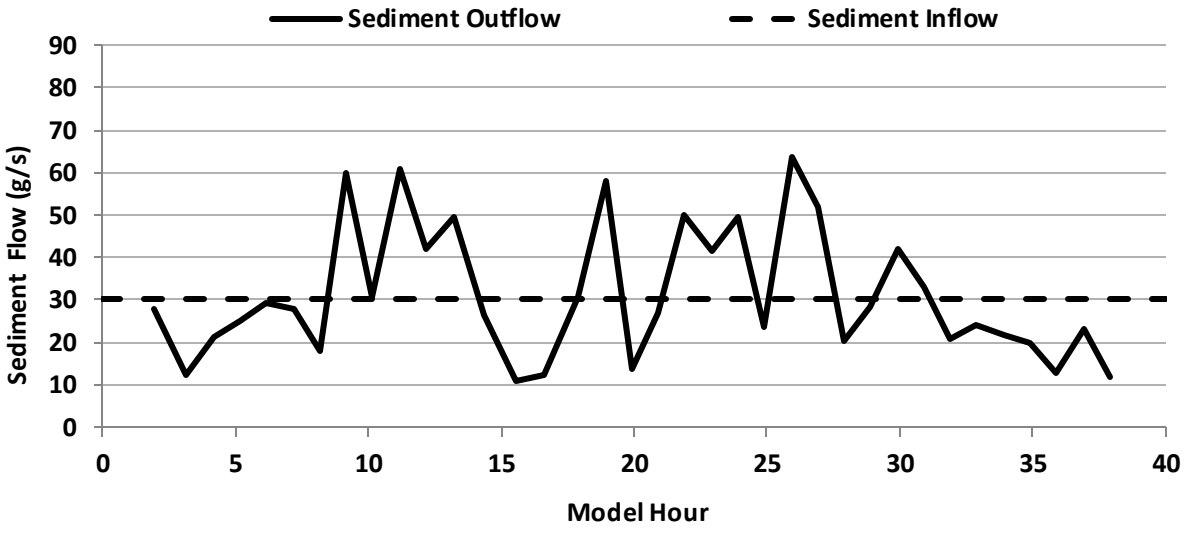

Figure 31: Run 2 sediment outflow measurements and averaged sediment inflow shown

The data collected during Run1 show that the run ended with an approximate total sediment outflow exceeding the sediment inflow by 1.06 m^3, indicating channel degradation. However, between model hours 5 and 20, the experiment was in a relative state of equilibrium indicated by the parallel cumulative plots of the sediment flow shown in Figure 28. The average sediment outflow during the testing was 47.46 g/s with a standard deviation of 21.92 g/s. It appears that most of the degradation

took part during the first 5 hours of the test, during which the highest sediment outflow of the experiment was recorded at 89 g/s. During the hours of 20 to 35, channel degradation occurred, coinciding with flow concentration along a wall of the flume.

The data collected during Run 2 show that the run ended with an approximate equal value of sediment inflow and sediment outflow, amounting to 0.03 m^3 of additional sediment outflow. Figure 30 shows that this balance occurred through several periods of aggradation and degradation, thereby demonstrating dynamic equilibrium. The averaged sediment outflow was 31.15 g/s with a standard deviation of 15.52 g/s. It should also be noted that the model was more stable during Run2 than Run1, reflecting fewer major fluctuations of sediment outflow.

5.3 Morphologic Data

This section presents observations and measurements regarding the morphology of the sub-channels forming the braided channel. The morphologic data were collected during Runs 1 and 2. The flow width ratio, explained in Chapter 4.4, was used to measure the morphologic data. Photographs used to show the observed braided morphologic features were taken from the fixed time-lapse camera and a portable Canon T3i camera. The observed features show some of the mechanisms involved in braided morphology evolution and sediment transport through the model.

5.3.1 Measured Morphologic Data

The measured morphologic data presented here show the variation of the flow width ratio during both runs of the experiment. The data are subsequently compared with the rate of sediment outflow from the flume. The following plots take into account the following aspects of the braided channel:

1. All cross sections, entailing cross sections 1-12;
2. The downstream half of the cross sections, entailing cross sections 7-12;
3. The downstream fourth of the cross section, entailing cross sections 10-12; and,
4. A comparison of items 1 through 3 mentioned above.

The different plots demonstrate that the channel's braided morphology continually changed along the flume during the two runs. It was observed, for example, that a low intensity of braiding recorded in the upstream section of the model did not necessarily imply that a low intensity of braiding occurred over the entire length of the flume. All plots presented here indicate values of flow width ratio measured for the downstream portion of the flume, because the behavior of the downstream portion of the channel is assumed to directly influence the measured rate sediment transport exiting the flume.

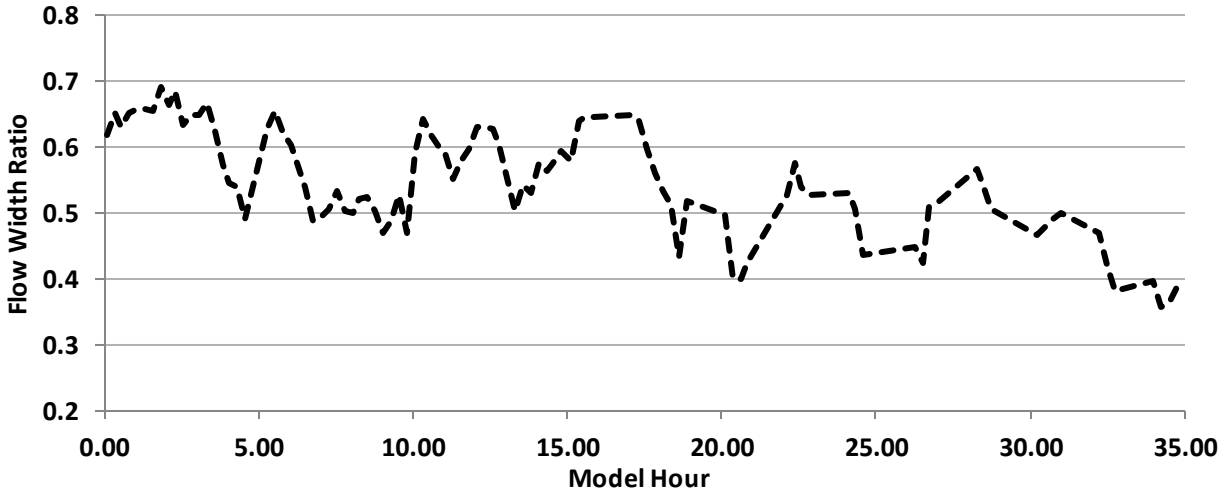

Figure 32: Run1 FWR with all cross sections accounted for (1-12)

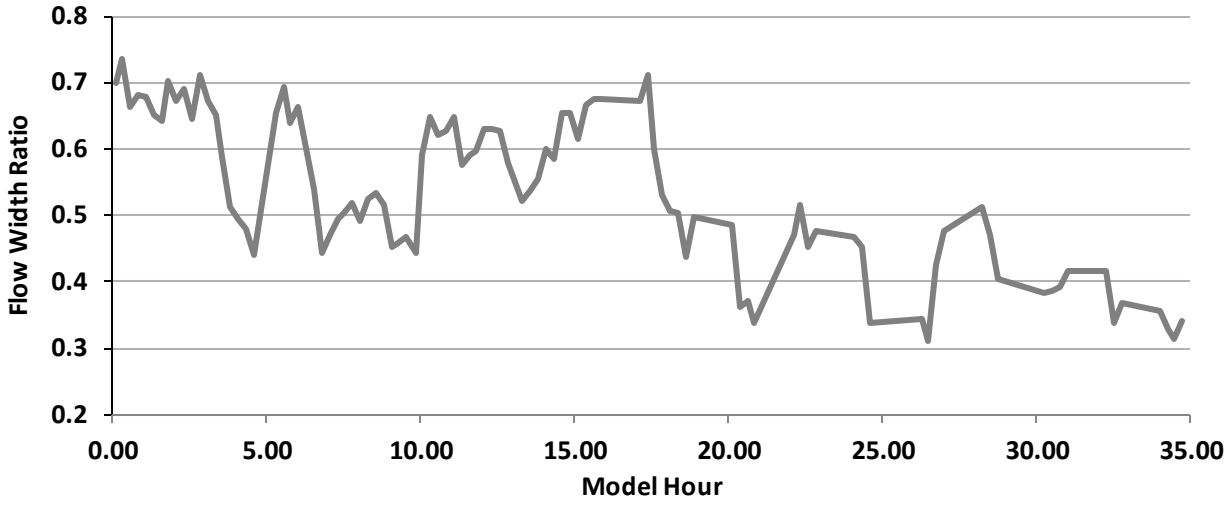

Figure 33: Run1 FWR with downstream half cross sections accounted for (7-12)

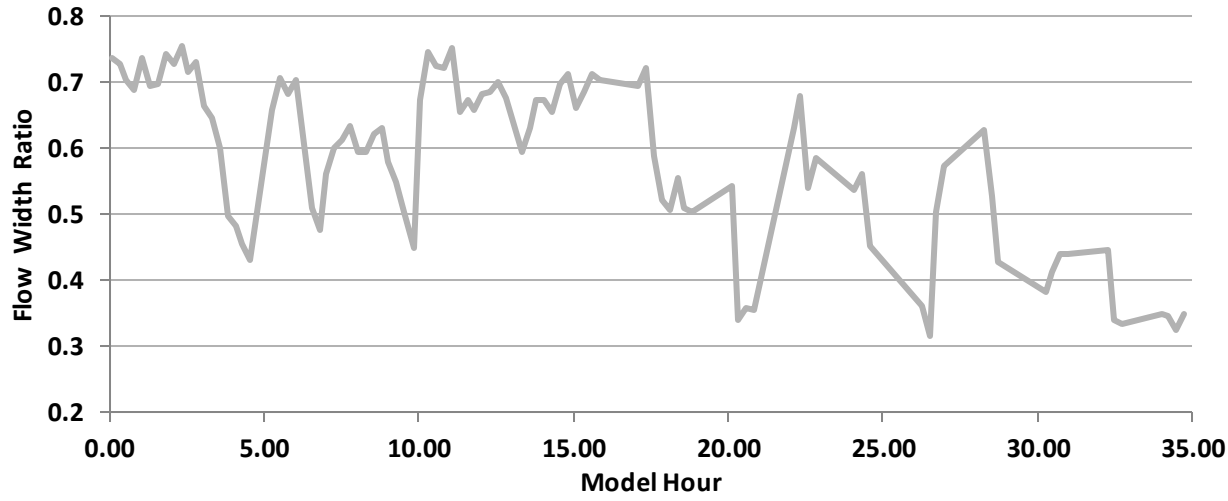

Figure 34: Run1 FWR with the downstream fourth of cross sections accounted for (10-12)

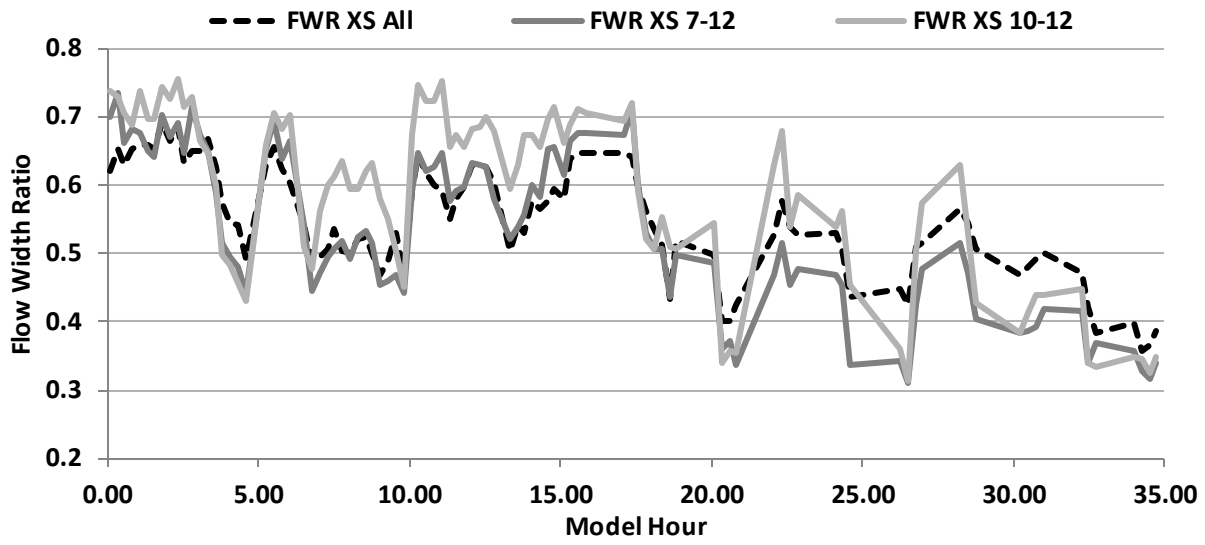

Figure 35: Run1 FWR shown with a comparison of different sections shown previously accounted for

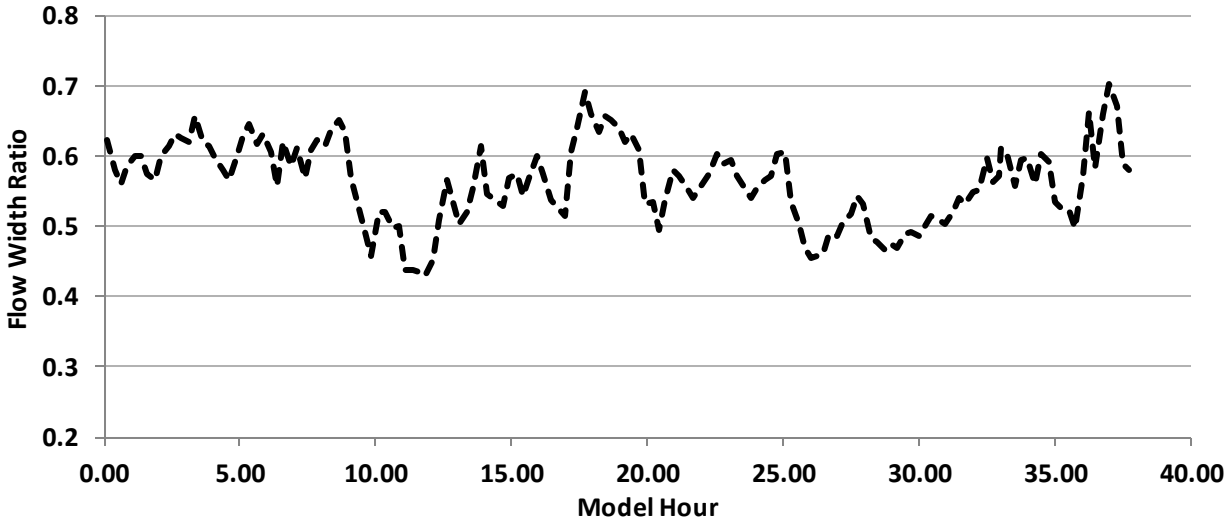

Figure 36: Run2 FWR with all cross sections accounted for (1-12)

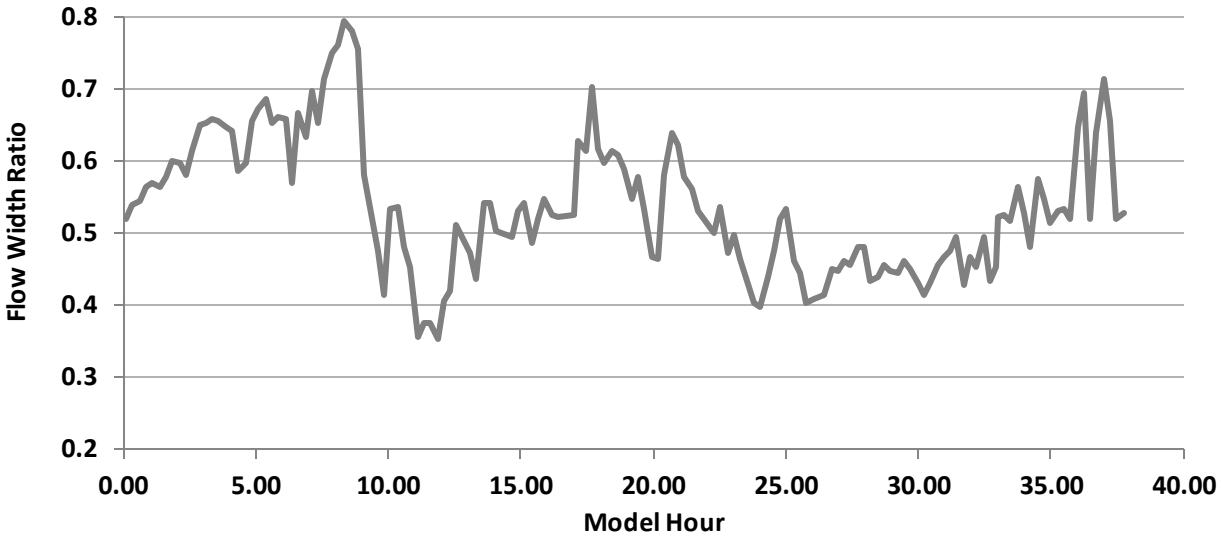

Figure 37: Run2 FWR with downstream half cross sections accounted for (7-12)

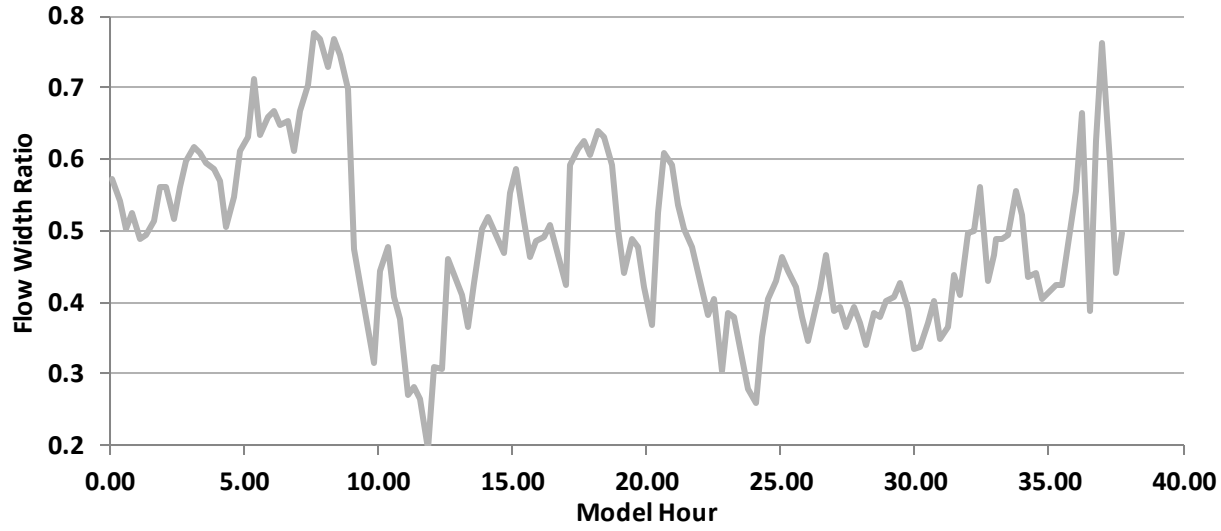

Figure 38: Run2 FWR with the downstream fourth of cross sections accounted for (10-12)

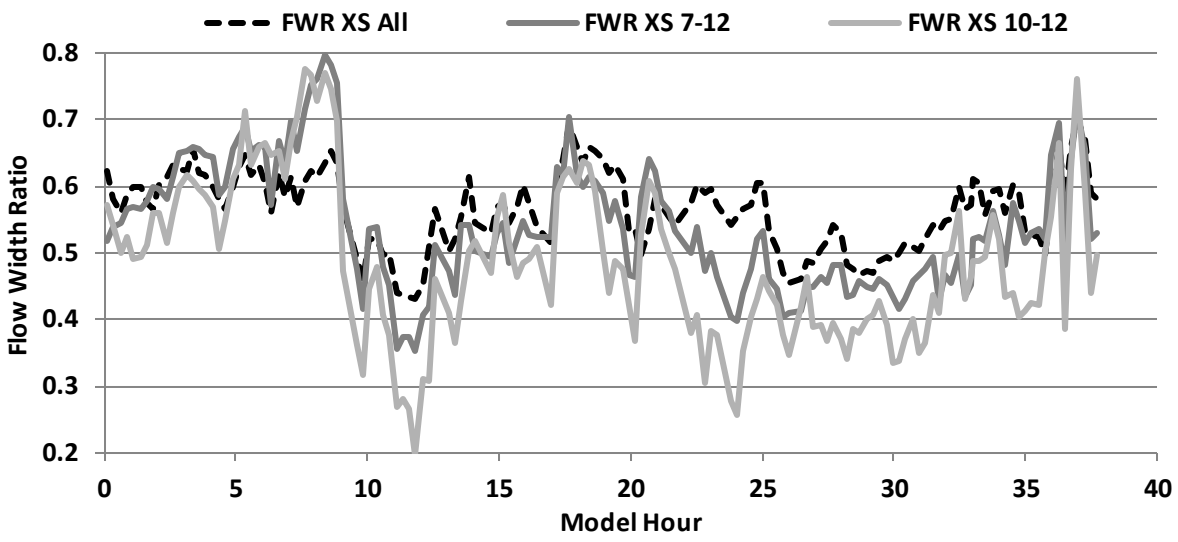

Figure 39: Run2 FWR shown with a comparison of different sections shown previously accounted for

The data in Figure 32-Figure 39 that the FWR fluctuated throughout the experiment, thereby demonstrating the dynamic nature of the braided channel morphology. They also indicate that the flow width ratio is useful in accounting for the dynamic nature of the model. During both Run1 and Run2, the data fluctuates around a median value of braided intensity of 0.5. FWR values higher than 0.5 indicated a higher braided intensity, whereas lower values indicate a lower braided intensity. The average value of FWR from Run1 accounting for all cross sections, for cross sections 7-12, and for cross sections 10-12 is 0.55, 0.53, and 0.58 respectively. Run1 had corresponding standard deviations of 0.08, 0.12, and 0.13. The averaged FWR from Run2 accounting for all cross sections, cross sections 7-12, and cross sections 10-12 is 0.56, 0.54, and 0.49 respectively. Run2 had similar corresponding values of standard deviations of 0.06, 0.09, and 0.12.

The streamwise connectivity of the braided channels during the experiment is best displayed in Figure 35 and Figure 39. These figures indicate the times when the braided channel showed a strong correlation between downstream and upstream braided intensity, and other times when the

streamwise braided intensity differed between the downstream and upstream sampling lengths. The figures also indicate that the downstream morphology, measured with FWR, is dampened when accounting for more cross sections of the reach. Meaning that the FWR values are more extreme when accounting for a smaller amount of cross sections, and average out to more median values when the FWR accounts for more cross sections. This demonstrates dynamic morphologic behavior both spatially and temporally. This result was more evident for Run2 than Run1, but the latter run still exhibits it. It is important to note times when the downstream morphology does not particularly match the entire reach because of the potential effect on the measured sediment transport. The sediment outflow was measured at the downstream section and therefore was most affected by the downstream morphology of the model. This dampening effect occurs at times when the downstream end had more flow width and times when the flow width was less than the upstream sections. This result shows that this observation was not a coincidence and that the model was sufficiently long enough to produce different morphologic behaviors at one time; both wide depositional sections of flow and also more concentrated degrading flow.

Another inference that can be made looking at Figure 32-Figure 39 is that local morphologic states never persisted for significantly long periods. If a section of high braided intensity or is highly inundated over the width of a cross section, it is almost certain that soon enough the section reverted back to a low intensity and continued to change back and forth over time. This reflected a dynamic equilibrium that exists in local morphology of braided rivers and is an important characteristic that defines them. For example, if a section of river was to stay in a constant state of low braided intensity, the increased flow concentration would lead to more defined channels and eventually become non-braided. However, this process was not seen to occur during the experiment for there was a constant local balance between low and high braiding intensities as well as streamwise balance of intensities in both Run1 and Run2.

5.3.2 **Observed Morphologic Data**

This section describes the morphologic behavior of the braided channel during the experiment. Included are findings from the flow width ratio plots presented in Section 5.3.1. Other figures demonstrate some of the known morphologic behaviors of braided rivers and rivers in general that was observed during the experiment. All of the figures presented below have implications on effects of sediment transport through the model and are used to explain relations between the morphologic data and sediment transport data collected and compared in Section 5.4.

The figures are presented here as photographs, either taken from the fixed time-lapse camera or from the mobile Canon T3i camera and are presented as follows:

1. Dynamic streamwise braided intensities;
2. Locally dynamic braided intensities; and,
3. Observed local morphologic mechanisms and processes in braided streams including:
    i. Main channels, anabranch channels, and bedforms
    ii. Bifurcations and confluences
    iii. Bar formation and decay

1. Dynamic streamwise braided intensities

Shown below are dynamic streamwise braided intensities existing longitudinally at one time, separated by a number of cross sections. Figure 40 shows the measured value of FWR from Run2 shown with several parts highlighted with corresponding photographs presented after. The times from the run that were chosen to demonstrate the dynamic nature of streamwise braised intensities and are labeled as follows:

a. Period of where the downstream braided intensity is larger than the upstream;

b. Period of where the downstream braided intensity is lower that the upstream; and,

c. Period of when the morphology was consistent throughout the length of the model.

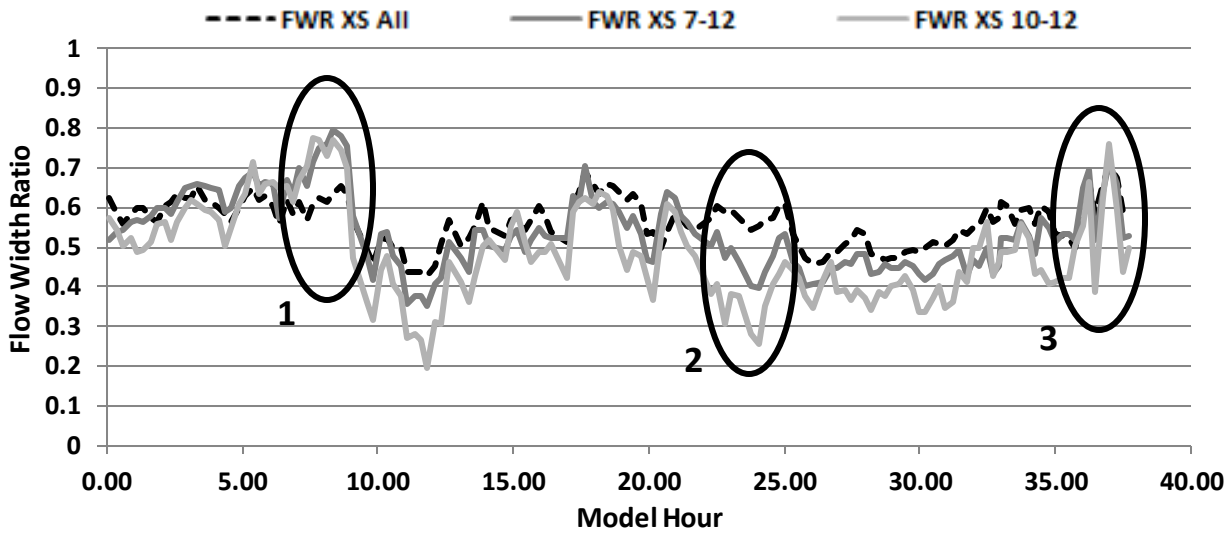

Figure 40: Measured flow width index from Figure 39 shown with 3 highlighted sections of different periods of morphologic conformity through the length of the model

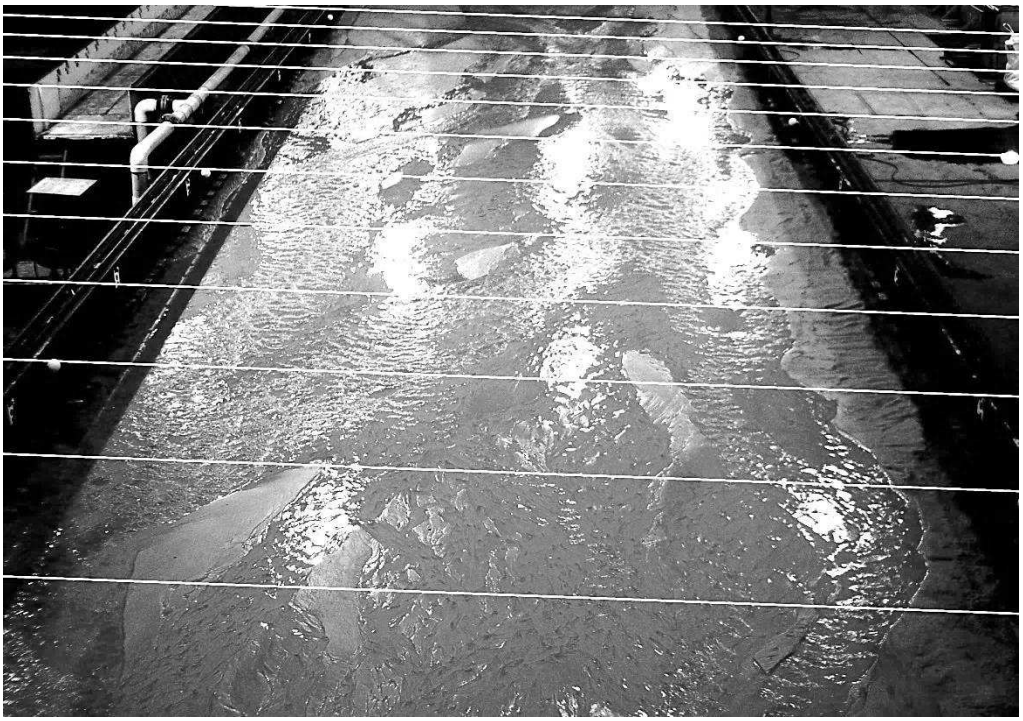

Figure 41: Shown above in Figure 40 as number 1, a time where a lower FWR was recorded in the upstream section than the downstream section. The transect lines are the cross-sections for FWR measurement

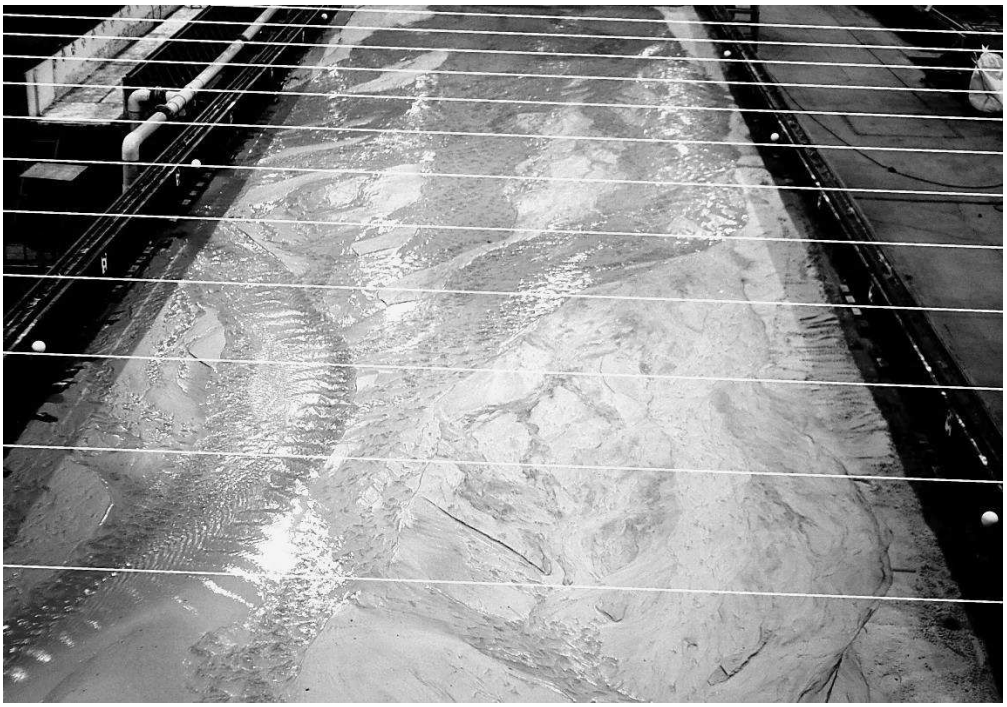

Figure 42: Shown above in Figure 40 as number 2, a time where a higher FWR was recorded in the upstream section than the downstream section

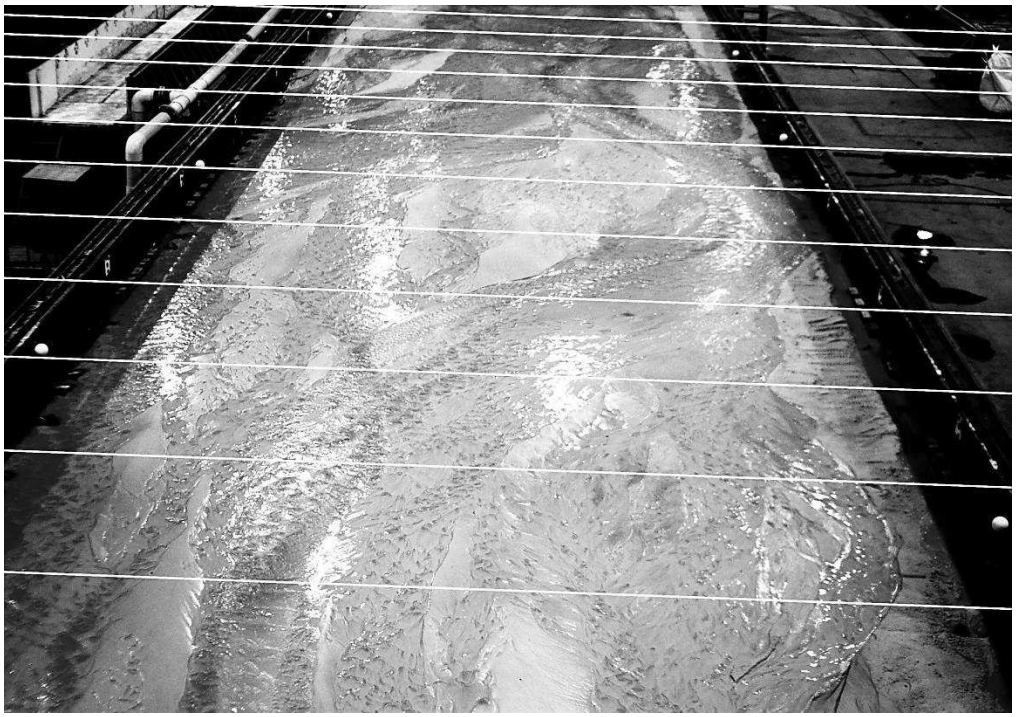

Figure 43: Shown above in Figure 40 as number 2, a time where a consistent FWR was recorded throughout the model

2. Locally Dynamic Braided Intensities

This section elaborates the local dynamic morphologic behavior that occurred during the experiment. Such dynamic behavior occurred along the entire braided channel, and no section of the channel tended to have a predominantly low or high value of FWR throughout the experiment. Even when a major anabranch was against the wall during Run1, periods of dynamic morphologic behavior were observed. The dynamic behavior is evident in Figure 44, which plots FWR values from the downstream fourth of the model during Run1, with a highlighted section during the last ten hours of testing showing a period of low to high then back to low braided intensity at the same location all within 6 hours. The corresponding views of the highlighted section of Figure 44 are depicted by the photographs in Figure 45-Figure 47. The downstream 3 cross sections correspond to the lower fourth of all the cross sections and match the data presented in Figure 44.

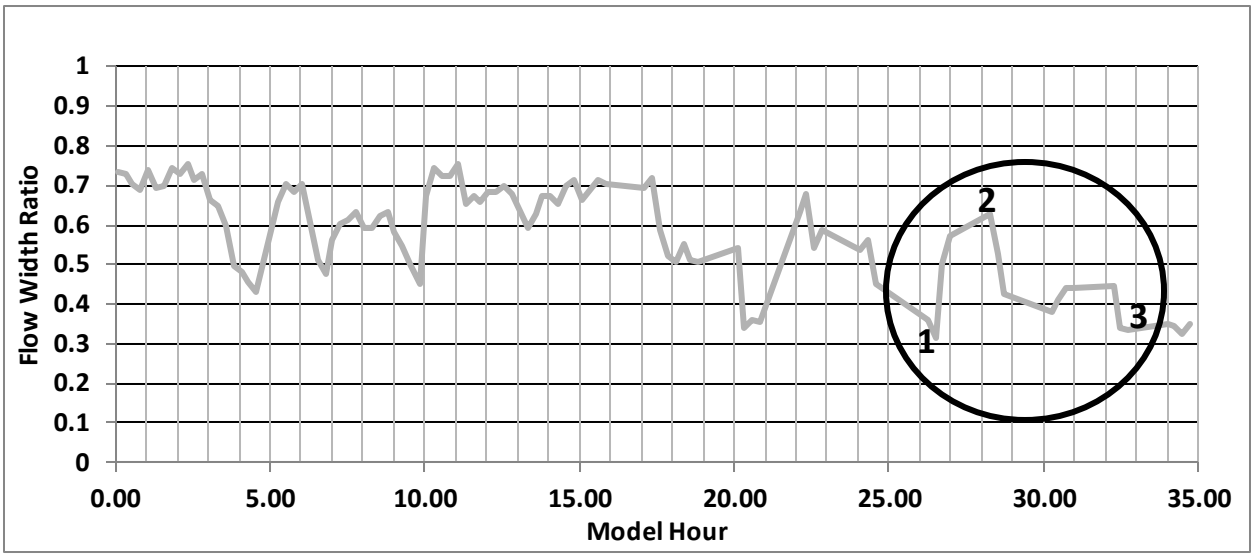

Figure 44: Measured flow width index from Figure 34 shown with a circled section of testing where dynamic local morphological behavior was witnessed

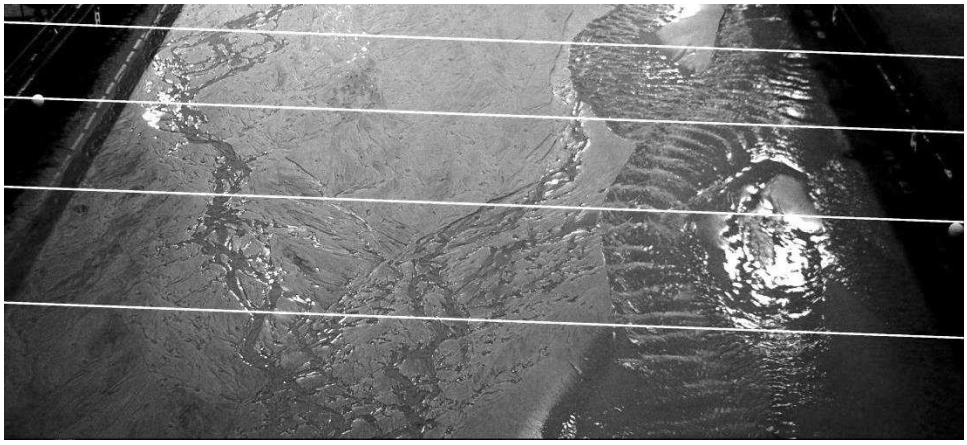

Figure 45: Shown in Figure 44 as number 1. Flow is from top to bottom

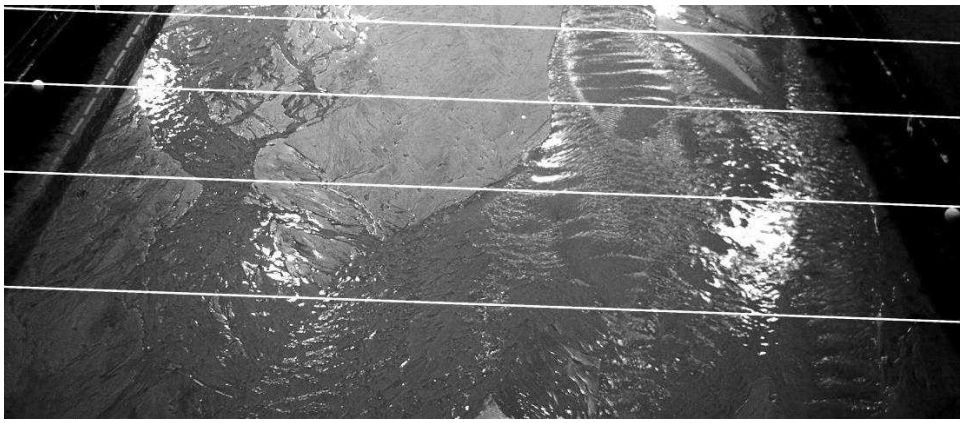

Figure 46: Shown in Figure 44 as number 2. Flow is from top to bottom

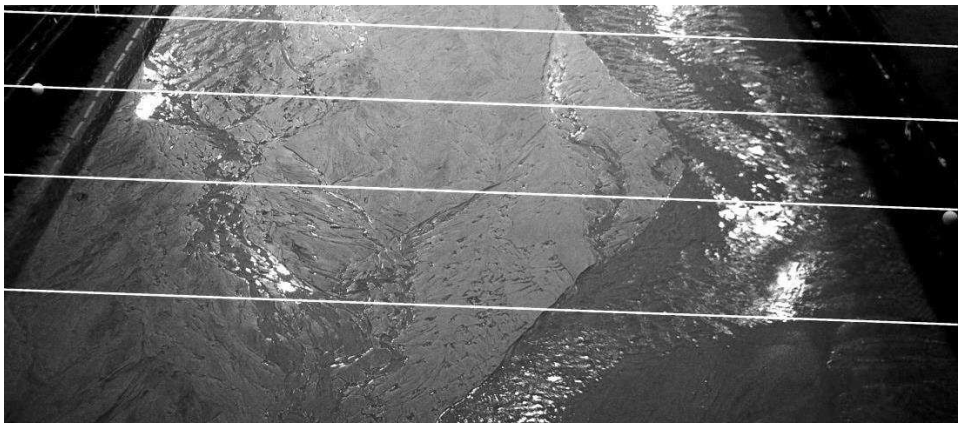

Figure 47: Shown in Figure 44 as number 3. Flow is from top to bottom

3. Observed Local Morphologic Mechanisms and Processes

   i. Main channels, anabranch channels, and bedforms

The movements of the component sub-channels (anabranches) of the braided channel interactively and continually shaped the overall braiding of the braided channel. While the main channels were visibly the primary source of sediment transport, the discharge required for them to exist occurred only when multiple anabranches converged. The predominant bedform of the main anabranch were anti-dune trains, while the smaller anabranches evolved a ripple or dune bedform. Figure 48 shows a period demonstrating the interaction between major and smaller anabranch channels. A fluorescent red color

was used to enhance the visual difference between the anabranches. When more flow passed through a section, the color was more pronounced; accordingly, the anabranch appearing more red was the dominant anabranch. However, the red dye also concentrated in quiescent areas, such as the lee of the ripples along some of the smaller anabranches. Additionally, some flow areas were not red, because they were either relatively small anabranches or were locations of sheet flow where flow spread at high speed over an advancing depositional bar.

It should also be noted that the main anabranches were not always as continuous as Figure 48 suggest. At times, more than one main anabranch existed, fewer trains of anti-dunes formed in them, and more anabranch bifurcations occurred. During these times, strong main anabranch divided into multiple smaller anabranches, sometimes reforming downstream if the smaller anabranches re-converged. Due to the relative shallow nature of all the channels and their non-cohesive banks, the continuous interactions of dominant and lesser anabranch channels was seen to be an important morphological process in the overall braided channel.

Figure 48: Main and lesser anabranches observed in the flume. Flow is from top to bottom

ii. Bifurcations and confluences

Bifurcations (or separation) and confluences (or convergences) of anabranches were observed throughout the experiment, and their basic morphological features played a major role in the dynamics of the braided channel. The two processes were closely linked and shaped some of the more well-known morphologic mechanisms and features observed in braided rivers. For example bifurcations seen in the flume were responsible for separation of flow and upstream migration of bars and islands. The bifurcations typically took shape of an alluvial fan that was deposited from a main channel or a strong anabranch that caused lateral separation of flow and thus formed a bar. A bifurcation is depicted in Figure 49.

Confluences enabled flow to increase along an anabranch, and were typically accompanied by a local region of confluence scour. When a confluence scour was large enough, flow depth and velocity through the anabranch downstream of the scour increased, thereby increasing anabranch size. Figure 50 shows a confluence of two anabranches and the confluence scour that formed. The red dye highlights the scour; as more red color indicates a deeper section where the flow converged.

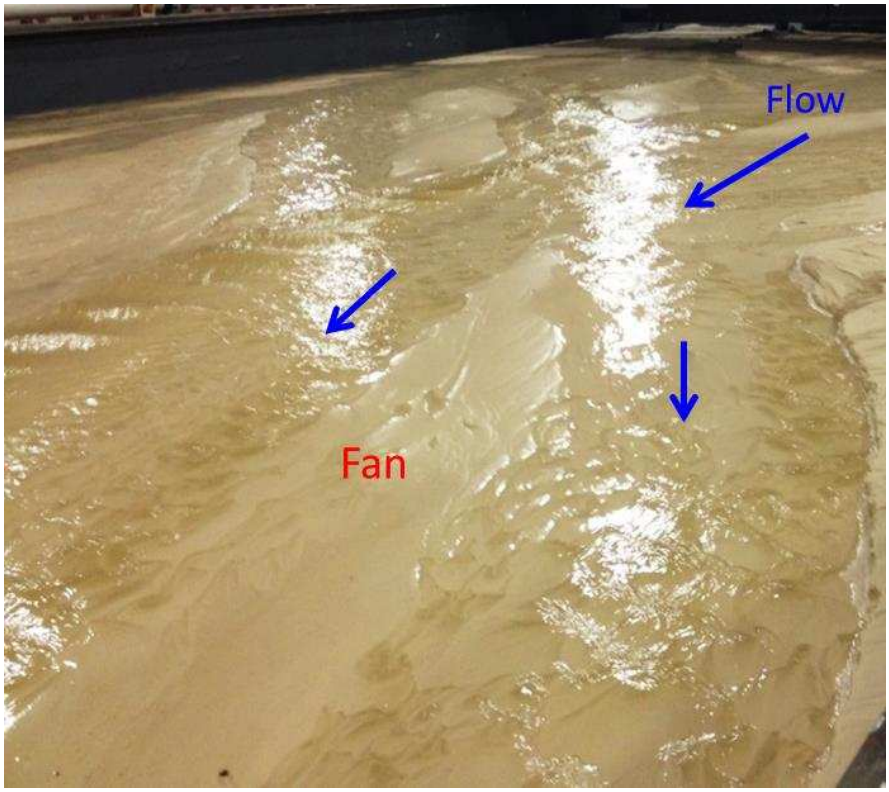

Figure 49: A depositional fan is formed at the end of a braid that then bifurcates

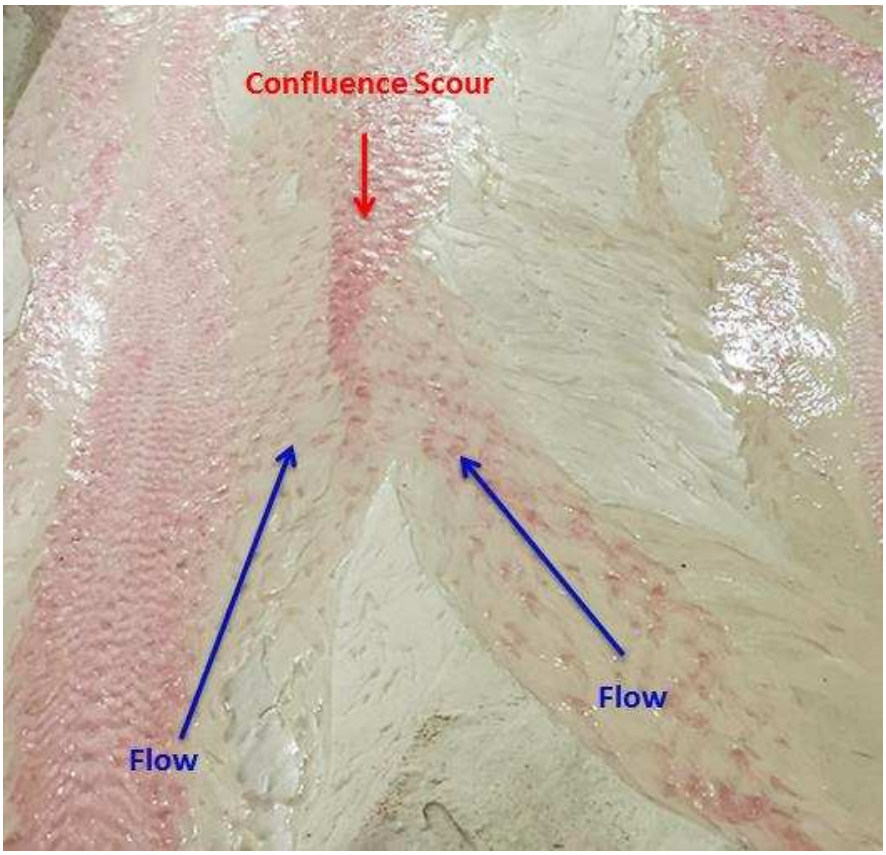

Figure 50: Observed confluence scour as two channels converge

iii. Bar formation and decay

Bar formation and development was witnessed throughout the both runs and significantly impacted the braiding pattern. Figure **51** is a set of photographs in taken at 15-minute intervals via the time-lapse camera and shows the evolving formation and eventual decay of a bar. The area of bar evolution is indicated by the red circle in each photograph. Figure 51a shows a main channel branch whose path crosses the highlighted circle area, the dominant anabranch is defined by its active anti-dune train. Figure 51b shows an anabranch with less flow and has dunes and ripples; it also shows the beginning of the emergence of a small bar inside the highlighted circle. Figure 51c-e show the progressive separation of flow around the emerging bar as can be seen by the lighter area of sand inside the highlighted circle. Figure 51f shows a now well defined bar now surrounded completely by smaller anabranches; also

evident is the appearance of a main flow channel, marked by the anti-dune train to the right of the bar. Figure 51g&h show the leftward lateral shifting of the dominant anabranch seen in the right of Figure 51f; this anabranch now began to erode the bar and forming vertical banks, as the anabranch grew. Also to be seen in Figure 51g&h is the decrease in water flow in the lesser anabranches surrounding the bar, because more of the flow was diverted to the dominant anabranch. Figure 51i shows the end of the cycle. By now most of the bar was being extensively eroded by the dominant anabranch, such that the sediment forming the bar was being transported downstream.

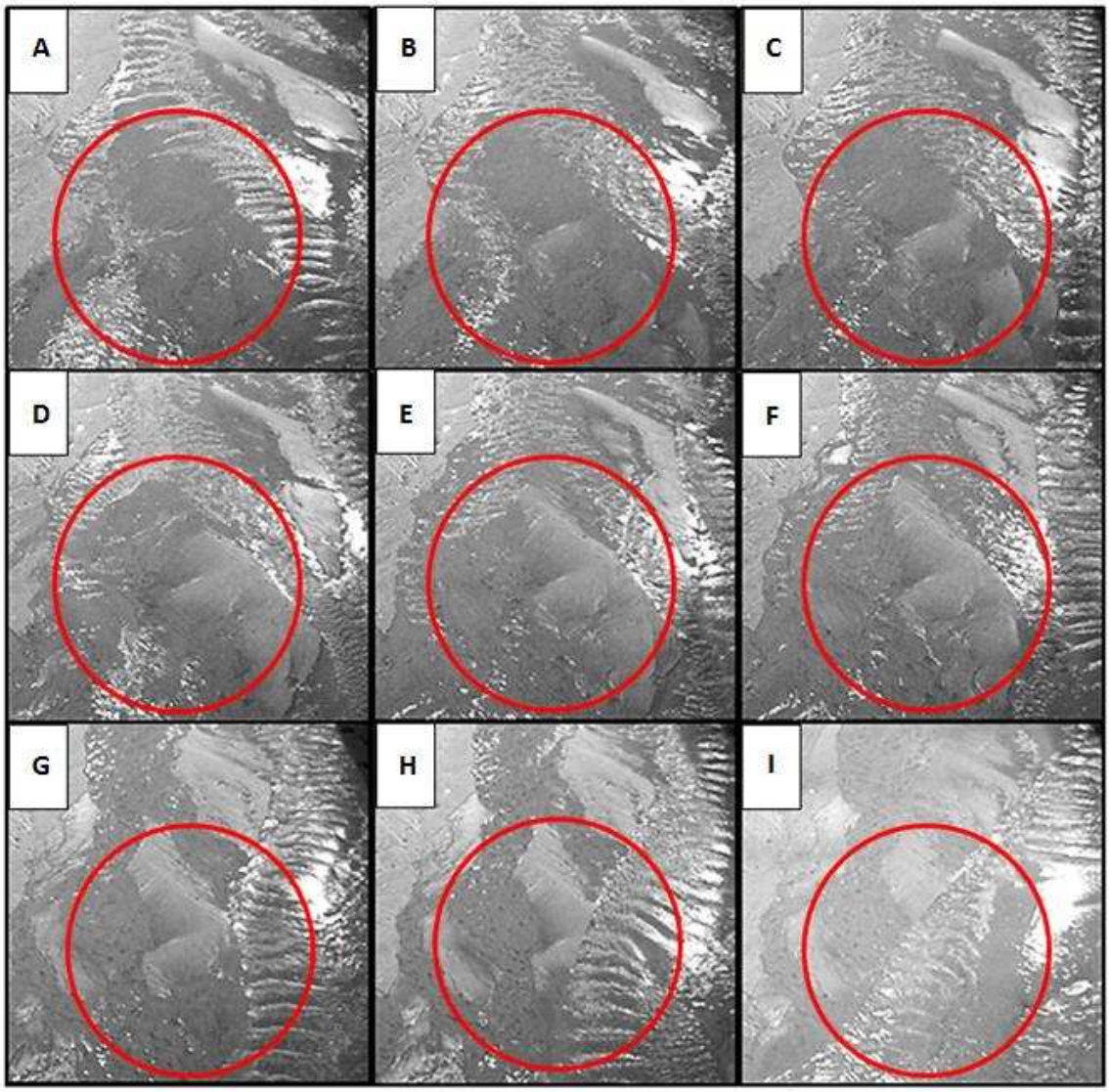

Figure 51: Bar formation and decay shown in sequential order with a time interval between each photo of 15 minutes, flow is from top to bottom

5.4 Sediment Outflow vs Flow Width Ratio Data

The following section compares the sediment outflow to the flow width ratio (FWR). The data are presented in various formats:

1. Time series (temporal variation) and discussion the of the morphologic index FWR versus rate of sediment flow from Runs 1 and 2; and,
2. Regression analysis of rate of sediment outflow versus the FWR.

The temporal variation of data are plotted as the rate of sediment outflow (left axis) and FWR values (right axis). Also shown on the plot is the rate of sediment inflow. Comparison of the in flow and outflow rates of sediment transport shows when sediment transport through the model attained an equilibrium balance. For convenience, an intermediate FWR value of 0.5 is plotted to coincide with the equilibrium sediment flow value to help give a visual comparison between the two variables. The scaling for each run differs slightly to match the values and include all the data measured.

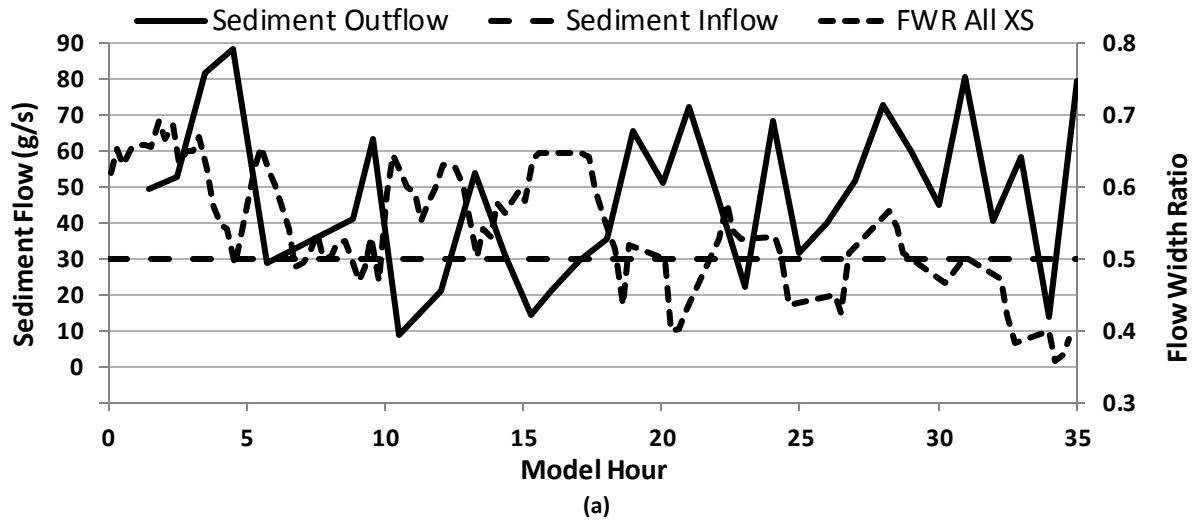

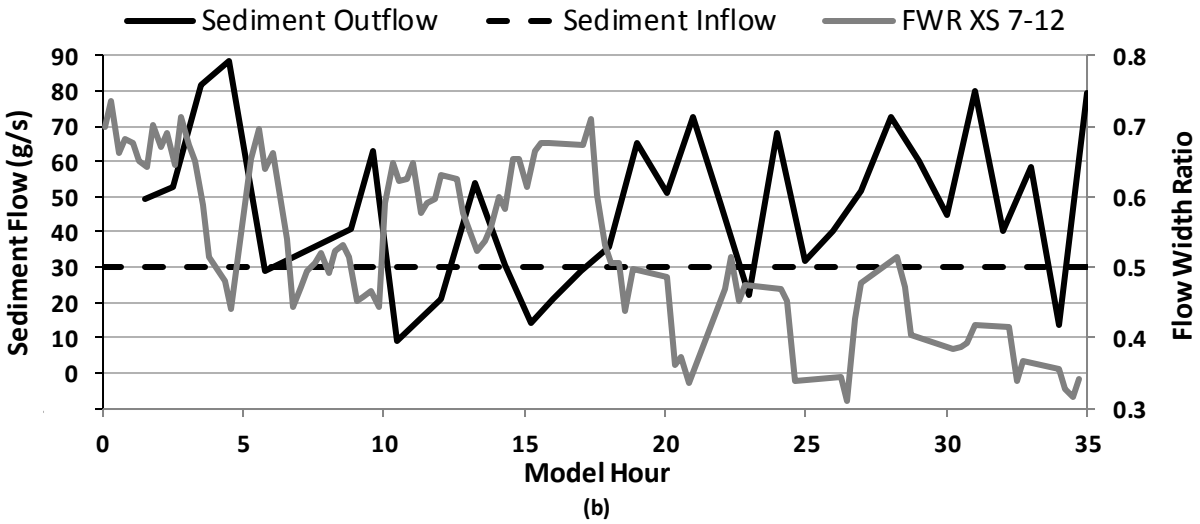

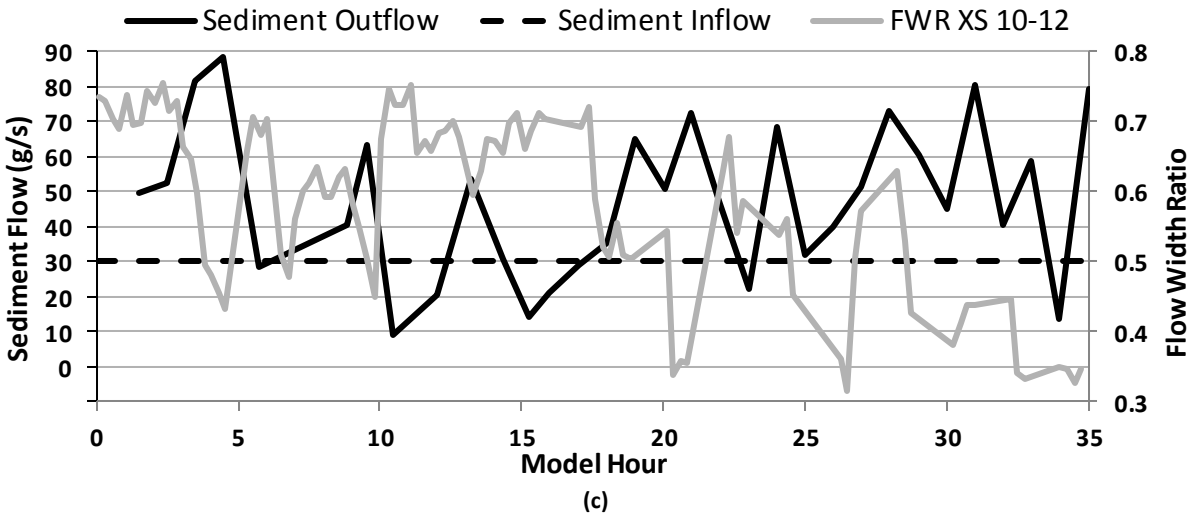

Figure 52(a)(b)(c): Run 1 sediment transport compared with the morphologic ratio FWR for various lengths of the flume

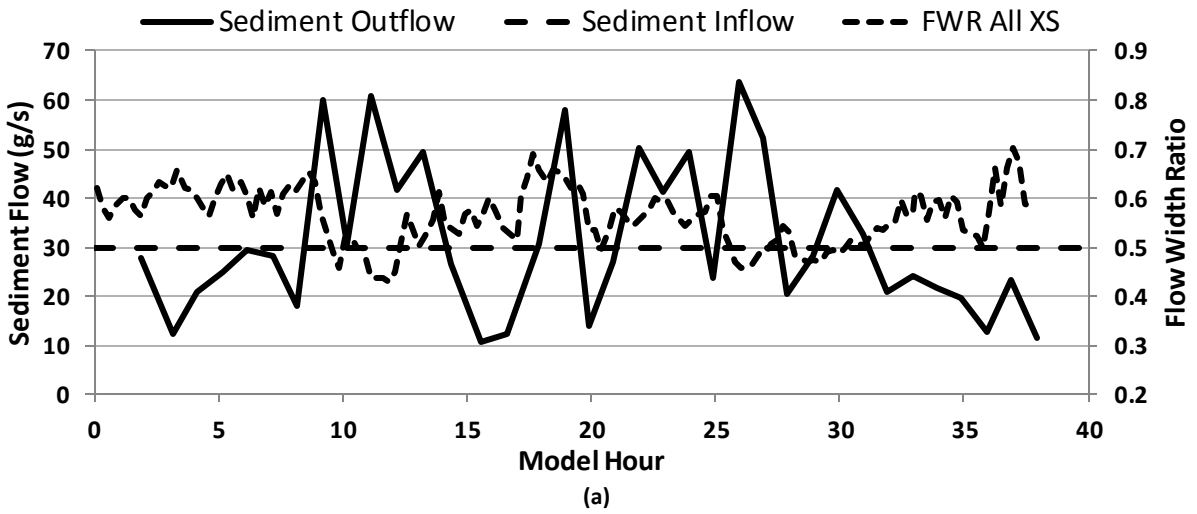

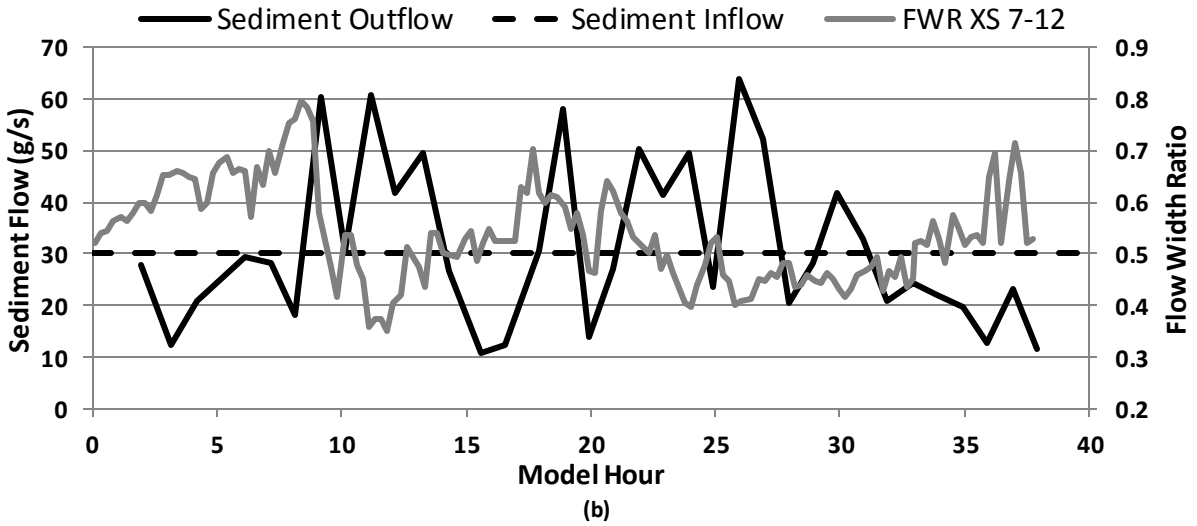

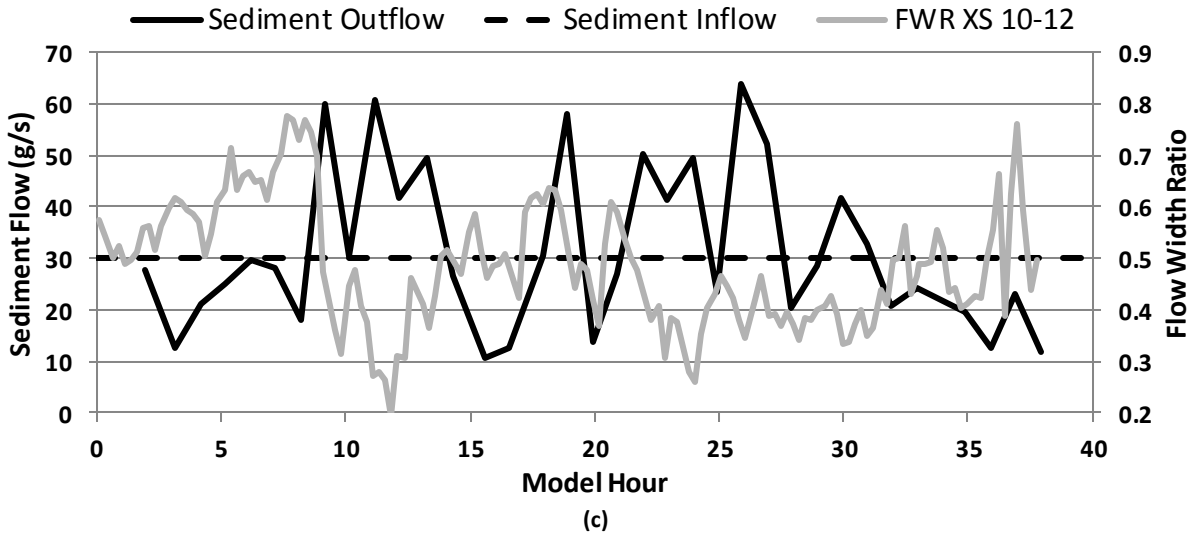

Figure 53(a)(b)(c): Run 2 sediment transport compared with the morphologic ratio FWR for various lengths of the flume

Figure 52 and Figure 53 show a semi-negative correlation between FWR and the rate of sediment outflow measured in the model. Having the sediment inflow match up with a median value of the flow width ratio, 0.5, usefully indicates how the data correlate. Generally, as the sediment outflow rate increases above the equilibrium value of 30 g/s, the flow width ratio falls below a value of 0.5 (and vice versa).. There are several contrasting periods in the plots that do not follow the inverse relation. However, it appears that the inverse relationship does become more apparent when the downstream morphology is weighted more heavily.

The values of FWR for the downstream morphology (cross-sections 10-12) are weighted more heavily in Figure 53(c) and Figure 54(c), than the FWR values for the entire flume or for cross-sections 1-12 in Figure 53(a)(b) and Figure 54(a)(b). The resulting correlation shows that the downstream morphology, the morphology closest to the measurement of the rate of sediment transport, affects the measured sediment outflow more-so than the overall morphology. This finding is important to note, and relates to the physics principle of locality; i.e., that an object (a bed sediment particle) is only directly influenced by its immediate surroundings. While the overall morphology of a braided channel characterizes sediment transport through the channel, local morphology affects the local rate of bed sediment transport.

The sediment outflow is then compared directly to the flow width ratio in a regression analysis. The comparison was done by quantitatively examining the trends in Figure 52 and Figure 53. While an approximate negative trend appears to exist, a regression analysis is a means to evaluate the strength of the relationship between the rate of sediment transport out of the reach and the FWR of portions of the reach. Each data point is rate of sediment outflow plotted against its corresponding value of FWR. Not every value of FWR was collected at exactly the same time as the sediment outflow measurements

(though they are close in time). Therefore, some FWR values are interpolated based on neighboring measurements of FWR. The regression analyses take part in two separate sets explained as follows:

1. Separate regression analysis of Run 1 and Run 2, and;
2. Combined regression analysis of Run 1 and Run 2 data.

The data is first presented separately to show the strength correlation of each individual run, and then looked at jointly to show a more comprehensive data set. Regressions from all previously examined reach lengths are also shown for comparison, i.e.; cross sections 1-12, cross sections 7-12, and cross sections 10-12.

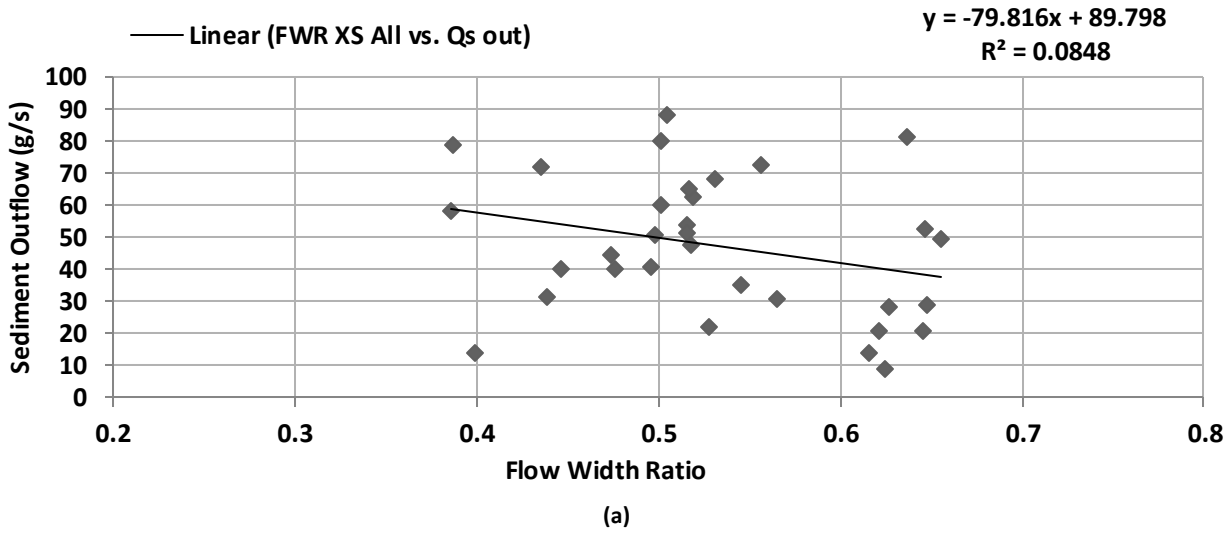

(a)

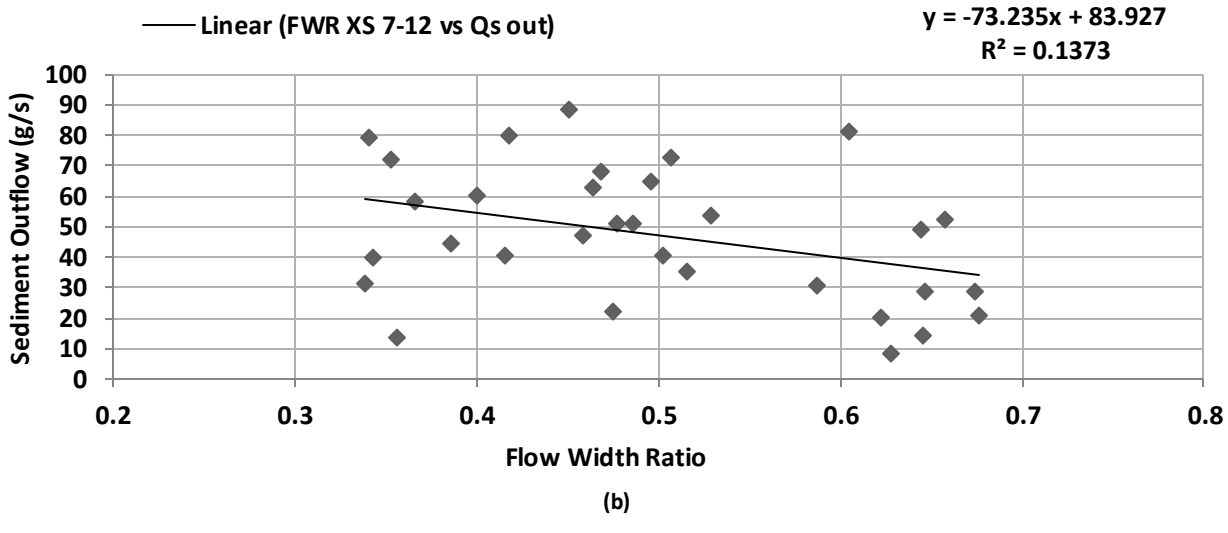

(b)

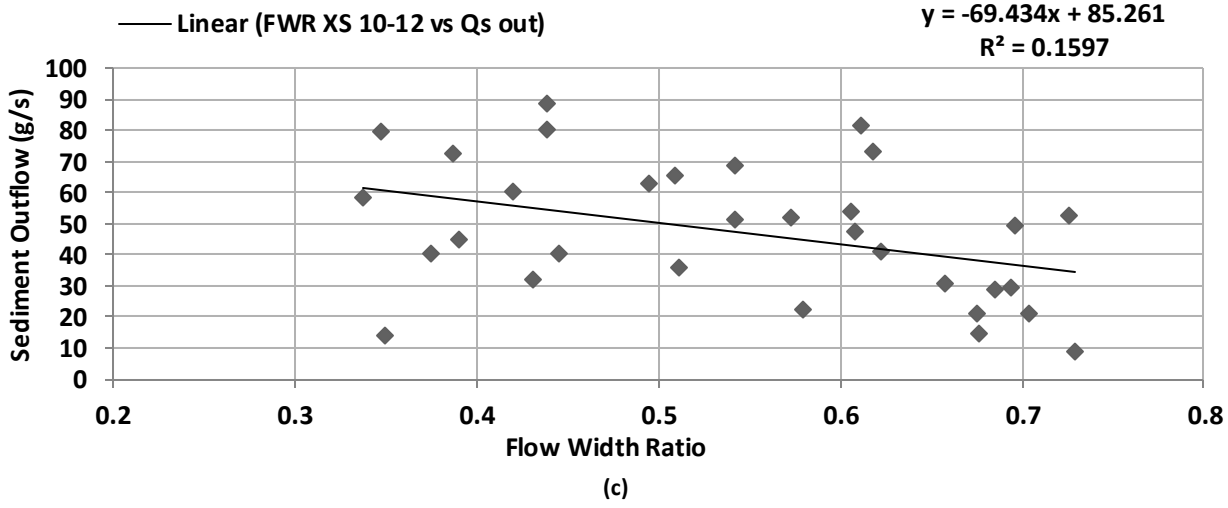

(c)

Figure 54(a)(b)(c): Run 1 Regression Analyses shown with the trendline equation and R^2 at top of chart

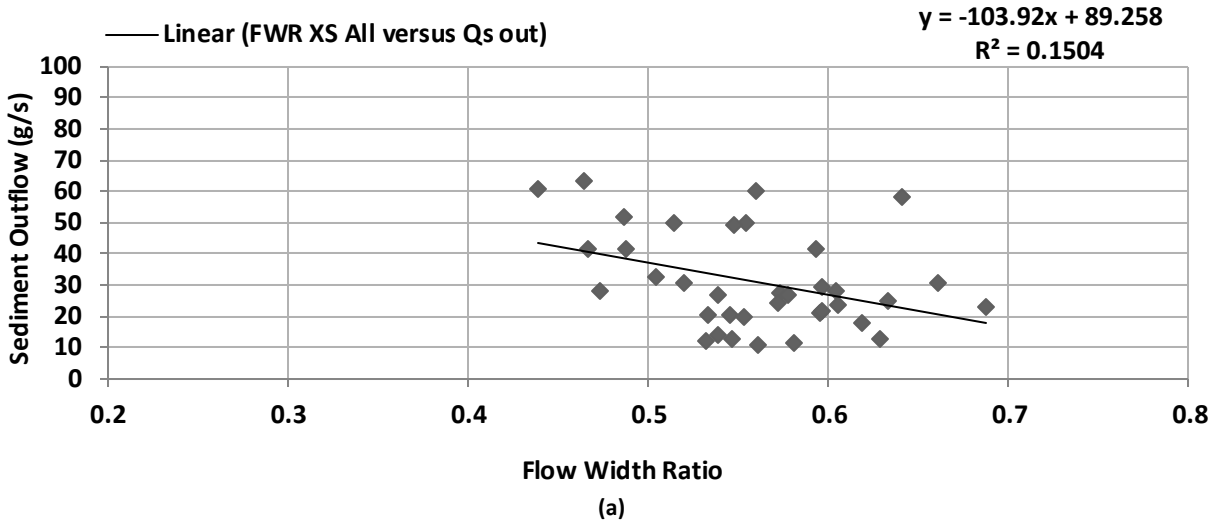

(a)

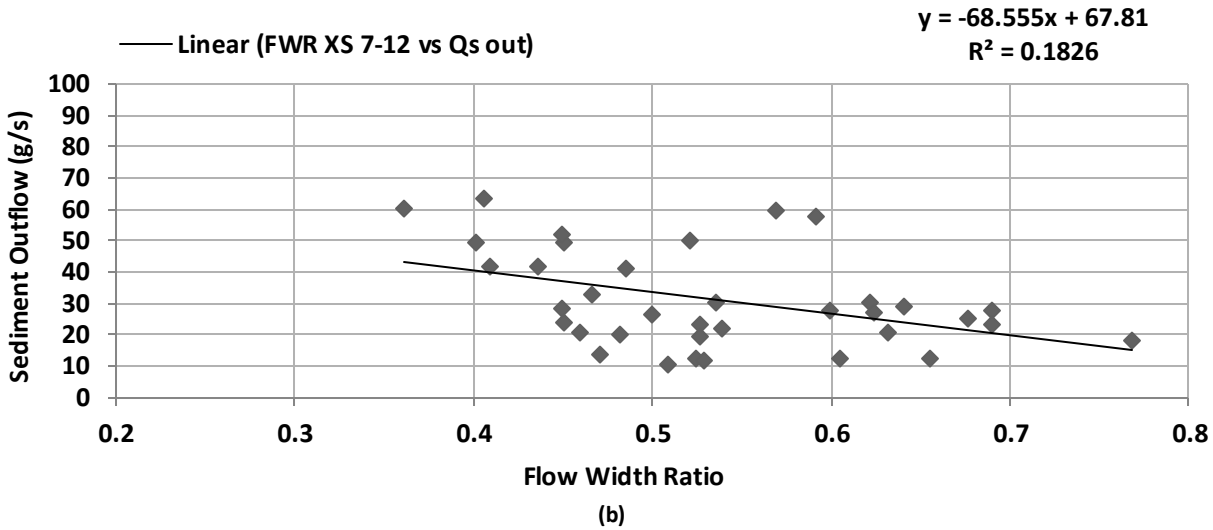

(b)

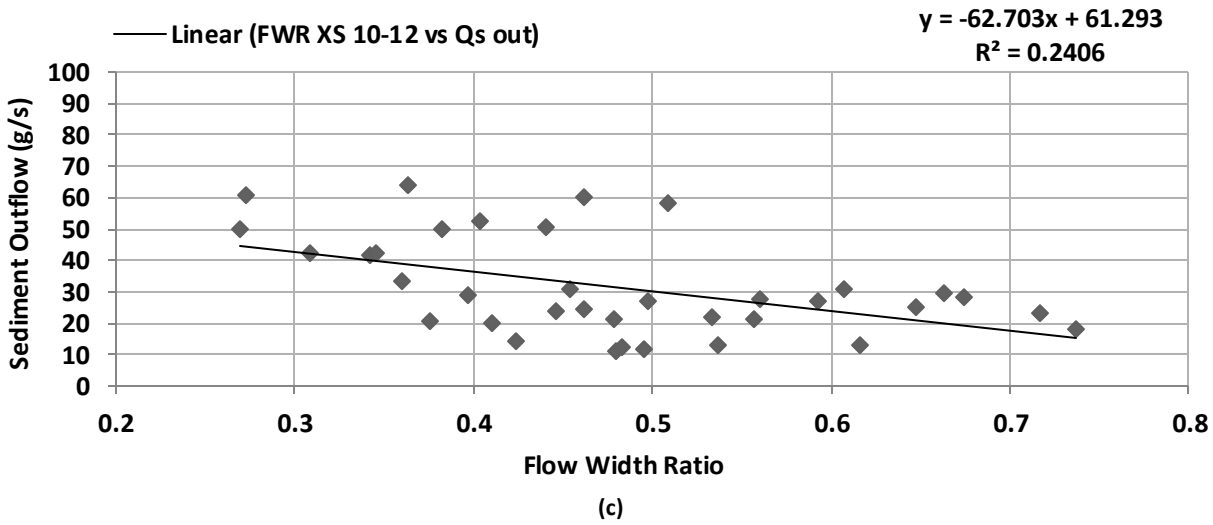

(c)

Figure 55(a)(b)(c): Run 2 regression analyses shown with the trendline equation and R^2 at top of chart

The separate regression analyses for Run 1 and Run 2, shown in Figure 54 and Figure 55, demonstrate the correlation strength between rate of sediment outflow and FWR for the runs independently. While there is a prominent variability in all the plots, there exists a negative correlation in all plots shown by the fitted trend-lines. The scatter of the data appears to be more pronounced in Run 1 data than in Run 2 data. Both runs have larger ranges of FWR values as the downstream sections are more heavily weighted. This demonstrates that local extremes in FWR values are dampened by including values from more cross sections. Also shown in the plots is an increasing R^2 value as the downstream sections are weighted more heavily. While the R^2 values from both Figure 54 and Figure 55 are low, further regression analyses revealed that all slope values, except Figure 54(a), were statistically different from zero (statistical significance is indicated by p values less than 0.05). The full range of the statistical findings for Run 1 and Run 2 are presented in Table 1 also reveals that the standard error in the slope estimate is reduced as the downstream section is weighted more heavily. Standard error is reduced as the extent of chance variation is reduced, meaning that there exists more confidence in the negative trend with the downstream regressions. This demonstrates that the principle of locality exists in the relation of the sediment transport and the FWR. Shown next is the results from the combined regression analyses.

Table 1: Regression analysis values presented from both Run 1 and Run 2

	Slope Estimate	Standard Error	R^2	p value
Run 1 XS All	-79.82	47.87	0.0848	0.1059
Run 1 XS 7-12	-73.24	33.52	0.1373	0.0368
Run 1 XS 10-12	-69.43	29.08	0.1597	0.0234
Run 2 XS ALL	-103.92	42.35	0.1504	0.0194
Run 2 XS 7-12	-68.56	24.87	0.1826	0.0093
Run 2 XS 10-12	-62.70	19.11	0.2406	0.0024

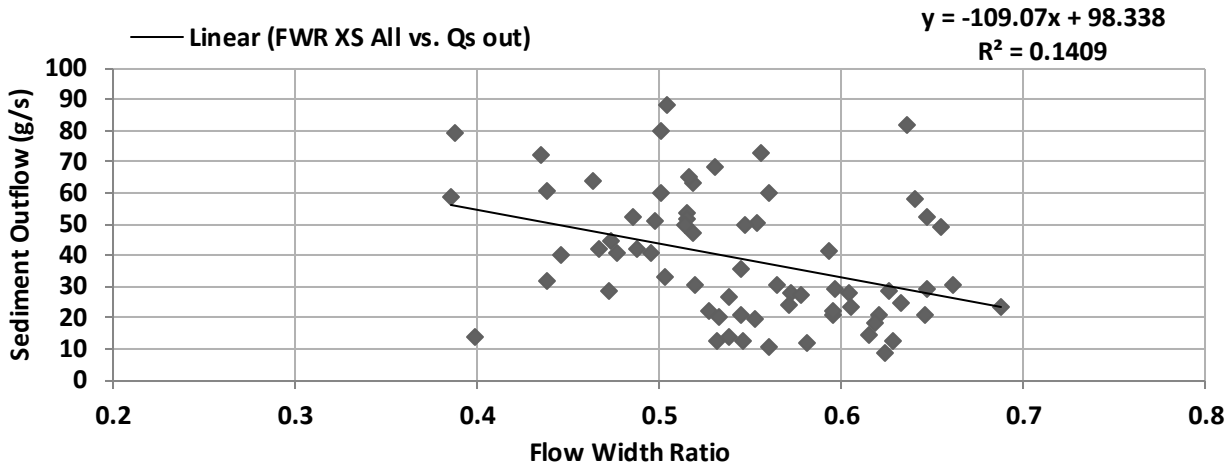

(a)

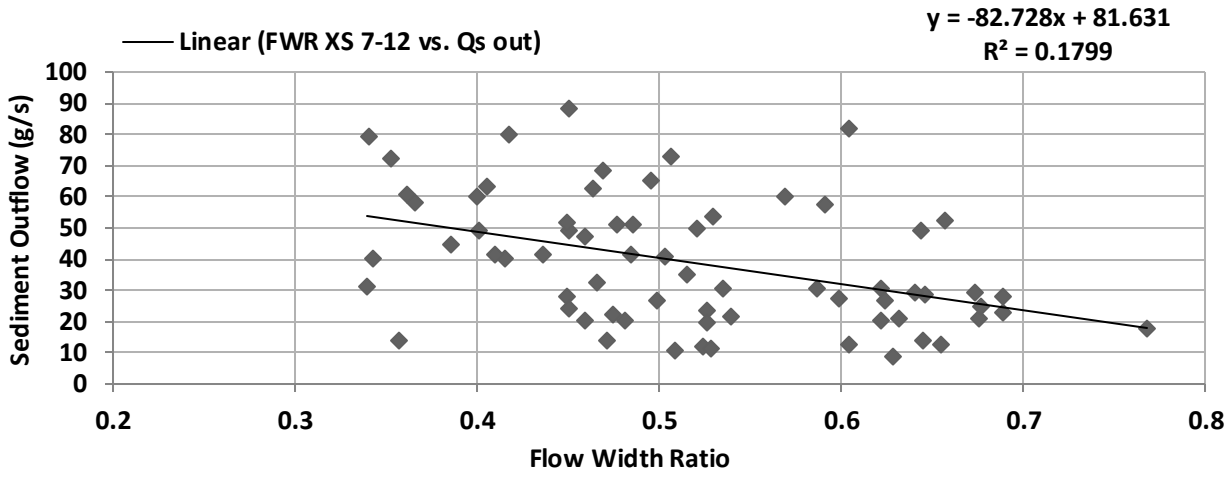

(b)

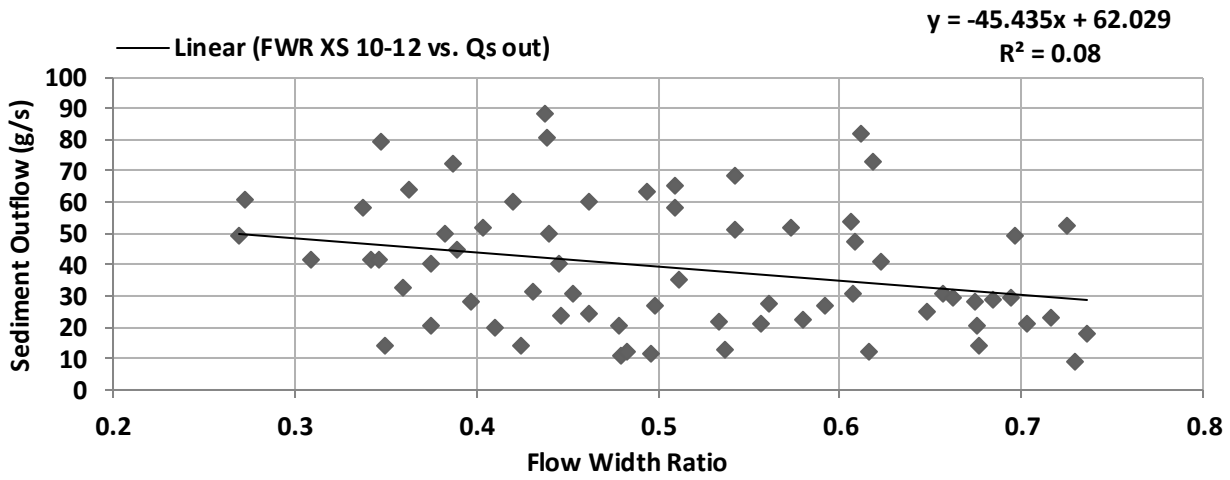

(c)

Figure 56(a)(b)(c): Combined regression analyses shown with the trendline equation and R^2 at top of chart

Combining the data from Runs 1 and 2 gives a more comprehensive data set for a regression analysis relating sediment outflow and FWR. The regression curves can be seen in Figure 56 and further statistical findings are presented in Table 2. The analyses of all the regressions from the combined data sets proved statistically significant with p values less than 0.05. While all plots are statistically significant there is still high variability in the shown by the scatter of the data in Figure 56. The stronger correlation (R^2 value) observed when weighting the downstream XS's that was observed for the runs separately is no longer observed when the runs are combined. This is contrasting to what has been shown before and should be noted. However, Table 2 also reveals that the standard error decreases as the downstream sections are weighted heavier as it did when the regressions were ran separately.

Table 2: Regression Analysis for the combined data from Runs 1 and 2

	Slope Estimate	Standard Error	R^2	p value
Combined XS All	-109.07	33.15	0.1409	0.0016
Combined XS 7-12	-82.73	21.74	0.1799	0.0003
Combined XS 10-12	-45.44	18.97	0.0800	0.0195

All plots from the regression analyses show a negative trend while also showing a fair amount of scatter. The variability evident in the plots comes from the inherently dynamic nature of braided channels, including both spatial and temporal variations in morphology and sediment transport. Table 3 shows the results from all the regression analyses together for convenience. This experiment only measured sediment outflow at the end of the flume, therefore it would follow that the measured downstream morphology would correlate more strongly with the sediment outflow measurements. This was shown in both separated regression analyses, but not in the combined regression when looking at the R^2 values. However, all the regression curves do have smaller standard errors when weighting the downstream morphology of the flume more heavily. In fact, the smallest standard error is that of the combined

regression when using the FWR from cross sections 10-12. All data from the regressions are shown together in Table 3.

Table 3: Data from all regression analyses shown together for comparison.

	Slope Estimate	Standard Error	R^2	p value
Run 1 XS All	-79.82	47.87	0.0848	0.1059
Run 1 XS 7-12	-73.24	33.52	0.1373	0.0368
Run 1 XS 10-12	-69.43	29.08	0.1597	0.0234
Run 2 XS ALL	-103.92	42.35	0.1504	0.0194
Run 2 XS 7-12	-68.56	24.87	0.1826	0.0093
Run 2 XS 10-12	-62.70	19.11	0.2406	0.0024
Combined XS All	-109.07	33.15	0.1409	0.0016
Combined XS 7-12	-82.73	21.74	0.1799	0.0003
Combined XS 10-12	-45.44	18.97	0.0800	0.0195

While general scatter in the data is present due to the variable nature of braided channels, some of the outlying data points can be explained through local morphologic mechanisms observed during the experiment. More on observed morphologic features can be seen in Section 5.3.2. . Figure 57 indicates outlying data values, with corresponding references to photographs that show local morphologic features involved.

Looking at the combined regression there are multiple points that stand out as outliers, however two points were chosen for discussion that do not match the inverse relationship between sediment outflow and the flow width ratio. Figure 57 shows the combined regression, for cross section 10-12, shown with projected standard error bars indicates the two outlying data points, labeled P1 and P2. Figure 58,Figure 59, and Figure 60 show photographs corresponding to the two data points. The points were chosen not only for being outside the standard error but also based on their disagreement with the negatively correlated trend. Both points are at least FWR = ±0.1 from a flow width ratio value of FWR = 0.5, to ensure the values represented moderate braiding or non-braiding intensity.

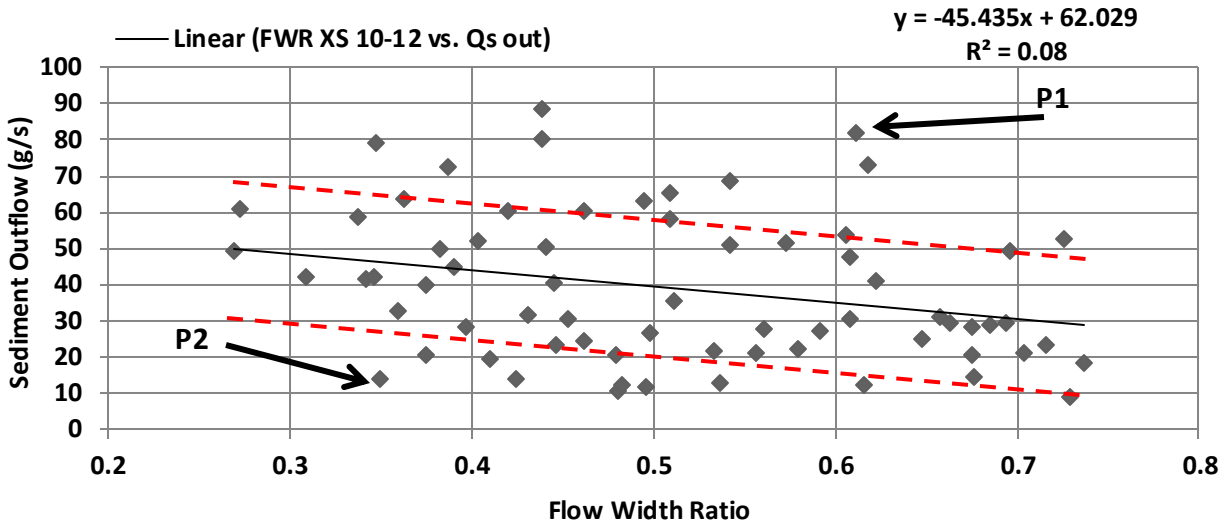

Figure 57: Combined regression analysis shown accounting for the downstream fourth of the flume, with outlying points labeled P1 and P2. The standard error is also projected on the plot shown as the dashed red lines.

For P1, FWR = 0.61, indicating moderately intense braiding. According to the suggested negative trend, moderately intense braiding should imply a moderately low rate of sediment outflow. However, the corresponding measured sediment outflow value was 81.76 g/s, an extremely high value for sediment transport through the flume. Shown in Figure 58 is the corresponding photograph from the point of data. The bottom three cross-sections shown by the white lines crossing the photograph help explain P1. A highly inundated downstream section is evident, but the bottom right of the photograph reveals a dominant anabranch, with strong anti-dunes, building a depositional bar just at the outlet cross-section. This morphologic development was accompanied by the relatively high value of sediment outflow measured during that time.

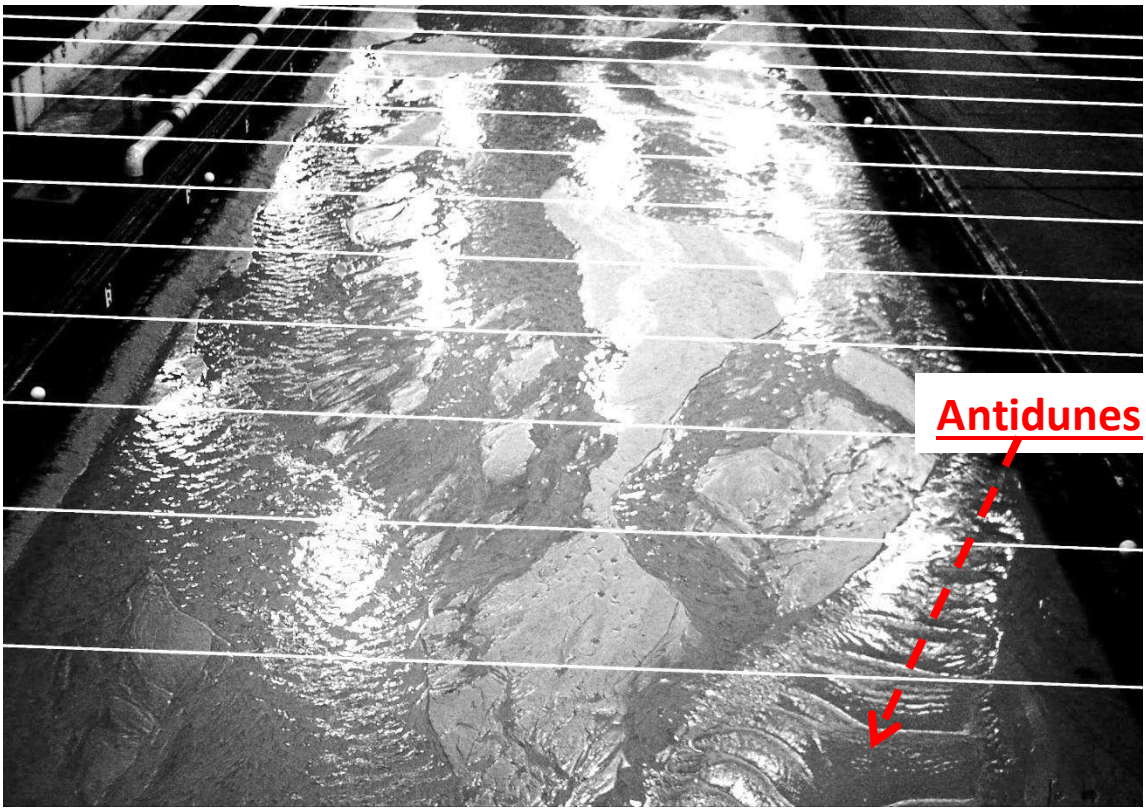

Figure 58: Photograph of flume corresponding to data point P1 in Figure 57. Flow is from top to bottom.

The outlying point P2, indicates a time when the measured rate of sediment outflow was uncharacteristically low, considering the relatively small value of FWR at the time. The sediment outflow value was 13.78 g/s, a rather low value, compared to when FWR = 0.348, a moderately low braided intensity value. During the measurements, a depositional bifurcation developed from a dominant anabranch that caused the formation and upstream migration of a bar, shown in the bottom right of Figure 59. A time-lapse series of photographs showing bar formation is presented in Figure 60 a-d; the bar formation is at the bottom right of the photographs. The sediment deposition occurred directly upstream of where the sediment flow was measured, thereby causing a momentary choking of sediment flow through the section, which resulted in the low sediment outflow measurement at that moment. The sediment measurement was taken at the 5:00PM (Figure 60a), suggesting that the beginning stages of bifurcation is highly depositional.

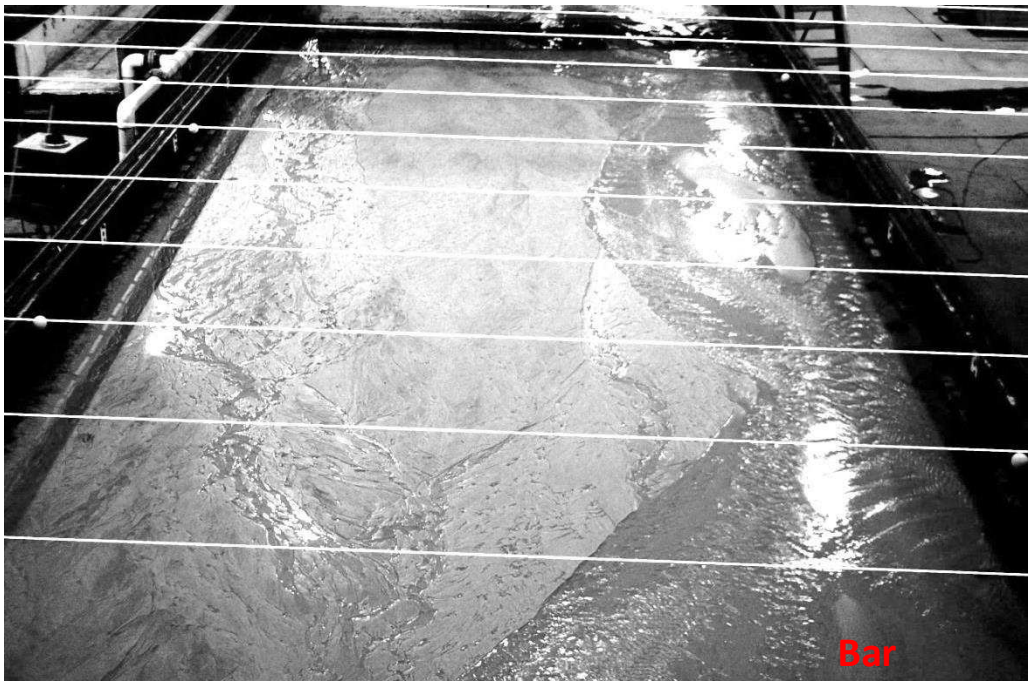

Figure 59: Photograph of flume corresponding to data point P2 in Figure 57. Flow is from top to bottom

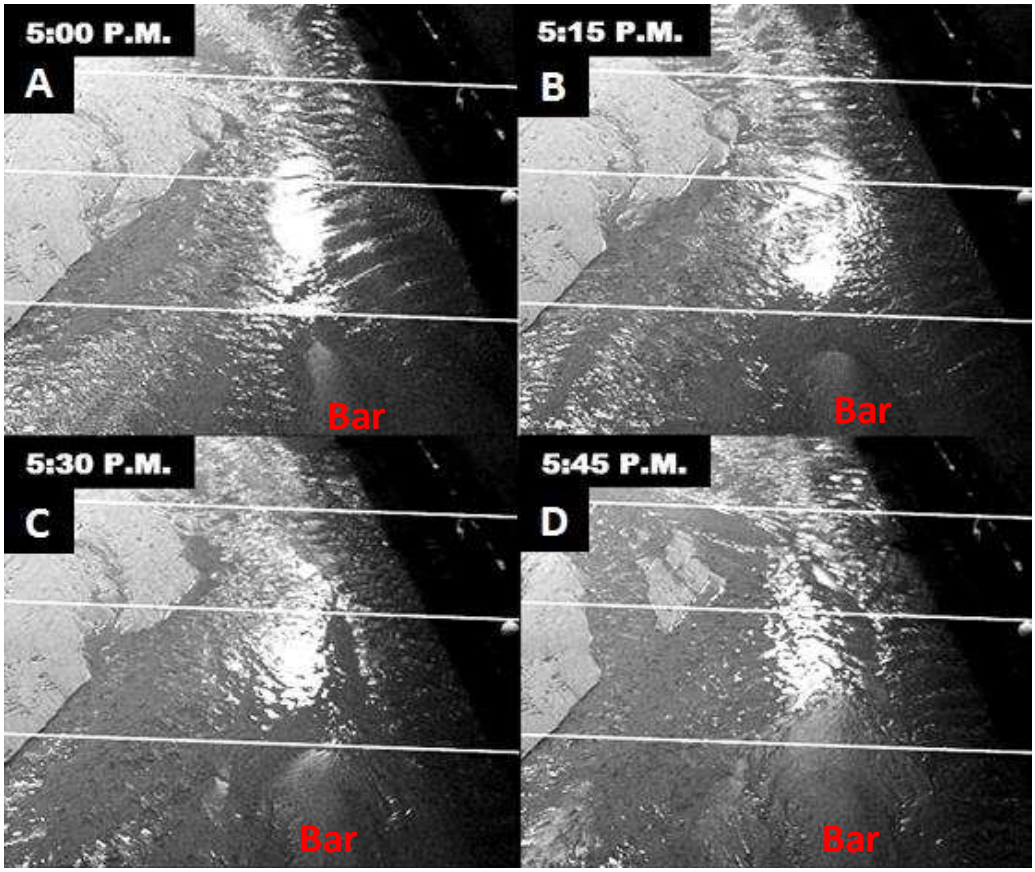

Figure 60: Time-lapse series of bar formation that lead to low sediment outflow measurement.

5.5 Further Discussion

This sections offers an explanation regarding the inverse relation between bed sediment transport and the braided intensity, measured via FWR. The explanation rests on fundamental relationships for shear stress and bed sediment transport.

Shear stress is the shear force per unit area exerted by the channel boundary by water (Arneson et al. 2013), and can be defined as follows:

$$\tau = \gamma R S_f \qquad \text{(Equation 8)}$$

Where: τ is shear stress (N/m^2),

γ is the unit weight of water (Kg/m^3),

R is the hydraulic radius (m), which is the cross-sectional area of flow dived by the wetted perimeter of flow,

S_f is the friction slope, or slope of energy grade line (m/m).

Conceptually, as the braided intensity is increased through a cross section the hydraulic radius decreased, due to the division of flow over the cross section into multiple anabranch channels that were shallow and wide in nature. The wetted perimeter increased as the number of channels increased, thereby making the hydraulic radius decrease. A decrease in hydraulic radius results in a decrease in channel bed shear stress (Equation 8), which consequently decreases the ability of the flow to transport sediment. Also for a given discharge, an increase in braided intensity and creation of more anabranches causes more flow contact with the bed surface. Overall, this trend increases hydraulic resistance to flow through the system, resulting in decreased velocities though the channels. Decreased overall or nominal velocity of flow, or decreased overall or nominal bed shear stress, reduces flow capacity to entrain and

transport bed sediment. It can be shown using a shear-stress excess relationship for bed-sediment transport (e.g., as in ASCE 2008) that these decreases, in turn, reduce bed sediment transport.

Due to the highly stochastic nature of braided systems, the flow paths are constantly affecting each other in unpredictable ways, meaning that fundamental sediment transport equations become less valid for explaining the full nature of sediment transport through their complex braided systems. Nonetheless, the fundamental relationships are useful for explaining the inverse relationship between bed sediment transport and FWR witnessed in this experiment.

6. Conclusions and Suggested Further Research

6.1 Conclusions

This thesis involved a flume experiment aimed at the following objectives:

1. Establish the parameters and procedure for establishing a braided channel along a flume;
2. Determine effective methods for measuring and relating bed-sediment transport and braided-channel morphology; and,
3. Ascertain how rate of bed sediment transport out of the reach contained along the flume relates to the morphology of the braided channel.

The calibrated input parameters used in this study led a braided channel to form in the flume. Effective methods were developed and used to measure both bed-sediment transport and braided channel morphology. The data and observations collected resulted in the following conclusions about braided channel morphology and rate of bed-sediment transport through them:

1. Braided river systems are spatially and temporally dynamic in nature, both in the way they transport bed sediment and in their morphology;
2. Although the rate of sediment inflow into the flume was steady, the rate of bed sediment transport out of the system was unsteady and fluctuated around a mean value when a time-averaged equilibrium of channel morphology existed. The dynamic nature of bed sediment transport out of the braided channel can be related to dynamic morphology of the braided channels;
3. The Flow Width Ratio (FWR) was a useful index for characterizing the changing morphology of the braided channel with steady flow conditions, and for relating bed sediment transport out of the system to the changing morphology. A regression analysis of the data indicate an inverse

relationship exist between the two aspects of channel behavior – as FWR increased, the rate of bed sediment outflow decreased; and;

4. Although the inverse relationship between FWR and measured bed-sediment transport existed over the entire length of the flume, regression analysis showed that the correlation became statistically more relevant when the downstream sections (closer to the cross-section of bed sediment measurement) were weighted heavier in the analysis. This finding demonstrates the well-known physics principle of "locality" whereby, for the present experiment, the movement of bed sediment particles were directly influenced only by their immediate surroundings. In other words, bed sediment transport is largely affected by local conditions of channel morphology and flow.

6.2 Suggested Further Research

The findings from this thesis present useful scientific methods that led to the identification of a statistically sound inverse relationship between bed-sediment transport and steady flow braided channel morphology. This relationship could be further explored by using the same methods applied to a more extensive amount of data; the present study developed 80 hours of experimental data.

In addition, FWR was a useful index for quantifying braided intensity for this study which used a steady flow scenario. However, further studies could explore FWR with sediment discharge through systems with unsteady flow conditions. This way the method could potentially be implemented for field use.

Also, data on bed sediment transport were collected at the downstream end of the flume. Further research could examine rates of bed sediment transport at multiple locations throughout the flume.

Such data would enable additional conclusions to be made about bed sediment transport and fluctuations in channel morphology along a braided channel.

References

Allen, J. (1952). Scale Models in Hydraulic Engineering. Longmans, London, Britain.

Arneson, L. A. et al. (2013). Evaluating scour at bridges (Hydraulic Engineering Circular No. 18). Washington, D.C.: Federal Highway Administration.

ASCE (2008). Sedimentation Engineering: Processes, Measurements, Modeling and Practice. Manual of Engineering Practice 110, ASCE Press, Reston, VA.

ASCE (2000). Hydraulic Modeling: Concepts and Practice. Manual of Engineering Practice 97, ASCE Press, Reston, VA.

Ashmore, P. E. (1982). "Laboratory Modeling of Gravel Braided Stream Morphology." Earth Surface Processes, Vol. 7, pp. 201–225.

Ashmore, P., & Egozi, R. (2008). Defining and measuring braiding intensity. Earth Processes and Landforms, 33, (pp. 2121-2138).

Ashworth, P. J., & Lane, S., & Widdison, P. E., (2010). Quantification of braided river channel change using archival digital image analysis. *Earth Processes and Landforms,* 35, (pp. 971-985).

Bertoldi, W., Welber, M., Mao, L., Zanella, S. and Comiti, F. (2014). "Flume Experiment on Wood Storage and Remobilization in Braided River Systems." Earth Surface Processes and Landforms, Vol. 39, pp. 804-813.

Bertoldi, W., & Tubino, M., & Zolezzi, G. (2006). Morphological analysis and prediction of river bifurcation. Department of Civil and Environmental Engineering, University of Trento, Italy. *Braided Rivers Process, Deposits, Ecology and Management.* (pp. 233-256).

Best, J., & Bristow, C., & Petts, G., & Sambrook, G. (2006). Braided rivers: where we have come in 10 years? Progress and future needs. University of Birmingham, Edgbaston, UK. *Braided Rivers Process, Deposits, Ecology and Management.* (pp. 1-10).

Bezzola, G., R., & Marti, C. (2006). Bed load transport in braided gravel-bed rivers. Laboratory of hydraulics, hydrology, and glaciology, Swiss Federal Institute of Technology, Zurich, Switzerland. *Braided Rivers Process, Deposits, Ecology and Management.* (pp. 199-215).

Bridge, J.S., & Lunt, I.A. (2006). Depositional models of braided rivers. Binghamton University, Binghamton, NY. *Braided Rivers Process, Deposits, Ecology and Management.* (pp 11-50).

Brogan, D., & Morgan, J., & Nelson, P. (2016). Application of Structure-From-Motion photogrammetry in laboratory flume settings. Department of Civil and Environmental Engineering, Colorado State University. *Geomorphology, Vol. 276 (pp. 125-143).*

Casado, M. C., & Gonzalez, R. B., & Kriechbaumer, T., & Veal, A. (2015). Automated identification of river hydromorphological features using UAV high resolution aerial imagery. *Sensors 2015, 15, (pp. 27969-27989).*

CENWP (2013). Detailed Performance Work Statement for Contract No. W9127N-10-D-0002, Alden Research & Laboratory Inc. Mount St. Helens GBS Physical Model, USACE.

Chandler, J. et al. (2002). Monitoring river channel change using terrestrial oblique digital imagery and automated digital photogrammetry. *Annals of the Assocication of American Geographers. 92:4, (pp. 631-644).*

Chipman, J. W., & Kiefer, R. W., & Lillesand, T. M. (2015). Basic principles of photogrammetry. *Remote sensing and image interpretation* (pp. 146-217). Hoboken, New Jersey: John Willey and Sons, Inc.

Chipman, J. W., & Kiefer, R. W., & Lillesand, T. M. (2015). Digital image analysis. *Remote sensing and image interpretation* (pp. 485-608). Hoboken, New Jersey: John Willey and Sons, Inc.

Dillabaugh, C. R., & Niemann, K. O., & Richardson, D. E. (2002). Semi-automated extraction of rivers from digital imagery. GeoInormatica, 6:3 (pp. 263-284).

Einstein, H. A., and Chien, N. (1954). "Similarity of Distorted River Models with Movable Beds." ASCE, Transactions, Vol. 121, pp. 440–457.

Ettema, R., & Armstrong, D. (2016) Hydraulic model study of grade building structures for the north fork of the Toutle River, Washington. Colorado State University Hydraulics Laboratory. Colorado State University

Franco, J. J. (1978). Guidelines for the Design, Adjustment and Operation of Models for teh Study of River Sedimentation Problems. Report H 78-1, US Army Corps of Engineers, Waterways Experiment Station, Vicksburg, MS.

Gessler, J., (1971). "Modeling of Fluvial Processes." Chapter 21 in: River Me chanics, H. W. Shen (Ed. and Publisher), Fort Collins, CO.

Gleason, G. L., & Smith, L. C. & Finnegan, D. C. (2015). Technical Note: Semi-automated effective width extraction from time lapse RGB imagery of a remote, braided Greenlandic river. *Hydrology Earth System Science,* 19, (pp. 2963-2969).

Graf. W. L. (1981). "Channel Instability in a Braided, Sand Bed River." Water Resources Research, Vol. 17, No. 4, pp. 1087-1094.

Hicks, D. M, & Lane S. N., & Westaway R. M. (2003). Remote survey of large-scale braided, gravel-bed rivers using digital photogrammetry and image analysis. *International Journal of Remote Sensing, 24, (pp. 795-815).*

Hoey, T. (1992). "Temporal Variations in bedload Transport rates and Sediment Storage in Gravel-Bed Rivers." Progress on Physical Geography, Vol. 16, No. 3, pp. 319-338.

Hoey, T. and Sutherland A. J. (1991). Channel morphology and bedload Pulses in Braided Rivers: a Laboratory Study. Earth Surface Processes and Landforms, Vol, 16, No. 5, pp. 447-464

Howard, A.D., Keetch, M. E. and Linwood, V. (1970). "Topological and Geometrical Properties of Braided Streams." Water Resources Research, Vol. 6, No. 6, pp. 1674-1688.

Hudson, R. Y., Herrmann, Jr., F. A., Sager, R. A., Whalin, R. W., Keulegan, G. H. Chatham, Jr., C. E., and Hales, L. Z. (1979). Coastal Hydraulic Models. Special Report No. 5, US Army Corps of Engineers, Coastal Engineering Research Center, Fort Belvoir, VA.

Hughes, S. A. (1993). Physical Models and Laboratory Techniques in Coastal Engineering. Advanced Series on Ocean Engineering, Vol. 7, World Scientific, Singapore.

Julien, P. (2002). River Mechanics. Cambridge University Press, Cambridge, Britain.

Kelly, S. (2006). Scaling and hierarchy in braided rivers and their deposits: examples and implications for reservoir modeling. Danish oil and natural gas Horsholm, Denmark. *Braided Rivers Process, Deposits, Ecology and Management.* (pp. 75-106).

Klaassen, G. J. (1990). "On the Scaling of Braided Sand-Bed Rivers." In: Moveable Bed Physical Models, H. W. Shen (Ed.), Kluwer Academic Publishers, Dordrecht, Netherlands, pp. 59–71.

Klaassen, G. J. (1992). "Experience from a Physical Model for a Bridge across a Braided River with Fine Sand as Bed Material." In: 5th International Symposium on River Sedimentation, Karlsruhe, Germany, pp. 509–519.

Kobus, H. (Ed.) (1980). Hydraulic Modelling. Bulletin No 7, German Association For Water Research and Land Development, Verlag Paul Parey, Munich, Germany.

Lane, S. L. (2006). Approaching the system scale understanding of braided river behavior. University of Durham, Durham. *Braided Rivers Process, Deposits, Ecology and Management.* (pp. 107-135).

Martins, R. (Ed.), (1989). Recent Advances in Physical Modeling. Kluwer Academic Publishers, Dordrecht, the Netherlands.

Moreton, D. J., Ashworth, P. J. and Best, J. L. (2002). "The Physical Scale Modeling of Braided Alluvial Architecture and Estimation of Subsurface Permeability." Basin Research, Vol. 14, No. 3, pp. 265–285.

Peale, A. C. (1879). Report on the Geology of the Green River District in Hayden, F.V. US Geol. And Geog. Survey Terr. 9th Ann. Rept. 720.

Pugh, C. A. (2008). "Sediment Transport Scaling for Physical Models." ASCE (2008). Sedimentation Engineering: Processes, Measurements, Modeling and Practice. Appendix C, ASCE Manual of Engineering Practice 110, ASCE Press, Reston, VA.

Rinaldo, A. and Rodriguez-Iturbe, I. (1993). "Self-Organized Fractal River Networks." Physical Review Letters, Vol. 70, No. 6, pp. 822-825.

Sambrook-Smith, G. H., Best, J. L., Bristow, C. S. and Petts, G. (2006). Braided Rivers: Process, Deposits, Ecology and Management. Blackwell Publishing Ltd., Oxford, UK.

Shen, H. W. (Ed.), (1990). Movable Bed Physical Models. Kluwer Academic Publishers, Dordrecht, The Netherlands.

Smith, G. S. (2006). Braided Rivers: where we have come in 10 years? Progress and future needs. School of Geography, Earth and Environmental Sciences, University of Birmingham, Edgbaston, UK. *Braided Rivers Process, Deposits, Ecology and Management.* (pp. 1-10).

USGS: Volcano Hazards Program CVO Mount St. Helens. Retrieved March 14, 2017, from https://volcanoes.usgs.gov/volcanoes/st_helens/st_helens_geo_hist_99.html

Warburton, J. (1996). "A Brief Review of Hydraulic Modeling of Braided Gravel-bed Rivers in New Zealand." New Zealand, Journal of Hydrology, Vol. 35, No. 2, pp. 157–173.

Warburton, J. and Davies, T. (1994). "Variability of Bedload Transport and Channel Morphology in a Braided River Hydraulic Model." Earth Surface Processes and Landforms Vol. 19, pp. 403-421.

Yen, B. C. (1999). From Modeling the Yellow River to Modeling of Rivers. International Journal of Sediment Research, Vol. 14, No. 2, pp. 85–92.